Structural Behavior of a Concrete Box Girder Bridge

RAYMOND E. DAVIS and JOHN J. KOZAK, California Division of Highways, and CHARLES F. SCHEFFEY, University of California, Berkeley

•DURING THE past three years the California Division of Highways and the University of California at Berkeley have carried out an extensive program of research pertinent to concrete box girder bridges. Although the program had a number of objectives, its primary goal was the study of the manner in which live loads are distributed transversely in a box girder. Secondary objectives involved the determination of: (a) dead load distribution, (b) influence of intermediate diaphragms on live load distribution, and (c) influence of barrier curbs and railings on live load distribution.

The University of California, in addition to providing consulting services in connection with the field test, conducted studies of models, including a small plastic model and a ¼-scale concrete model of the prototype. The program also included a study of analytical methods which might accurately describe the empirically determined behavior of the structure.

The box girder section is generally conceded to have high torsional rigidity with attendant efficient transverse distributional properties. There is, however, a lack of experimental evidence and analytical procedures which can produce quantitative answers to support design specification provisions for load distribution.

SCOPE

The principal experimental effort comprised the field test of a new structure on the State highway system, the Harrison Street Undercrossing, in Oakland, Calif. This structure was instrumented with SR-4 electrical resistance strain gages, Carlson strainmeters, and deflectometers to permit measurements of longitudinal and transverse strains and girder deflections resulting from a dynamic loading provided by a heavily loaded R-15 Euclid dump truck. Tests were conducted first without an intermediate diaphragm, secondly with a single intermediate diaphragm, and then after the addition of curbs and barrier railings.

Strains and deflections produced by the slowly moving test vehicle were recorded by oscillographs housed in an instrumentation trailer parked beneath the structure. Companion tests were conducted and supplementary instrumentation was provided to support the principal objectives and investigate secondary objectives, among which were the following:

1. Control tests were accomplished concurrently with the dynamic testing to evaluate physical properties of the component materials of the structure. Tests were conducted on four concrete control beams, on standard concrete cylinders, and on reinforcing steel coupons.
2. Laboratory tests were conducted by the University of California on a plastic model of 1/30-scale and a concrete model of ¼-scale.
3. A small amount of dynamic testing was performed, with the test vehicle traversing the structure at speeds of 5, 10, 15, and 20 mph and with various patterns of obstruction on the structure and its approach. In addition to selected strains and deflections, the accelerations of the structure and test vehicle were measured. This phase of the test was not included in original plans for the program and is not discussed here; however, it was considered a worthwhile adjunct to provide valuable information per-

Paper sponsored by Committee on Bridges.

tinent to impact effects on box girders for later use, when existing instrumentation permitted acquisition of the data at little additional expense.

4. Certain supplementary instruments were included within the structure to provide information concerning shears and temperature distribution. These included a group of thermocouples and five shear rosettes. Also, because of the questionable nature of the information provided by some of the internal gages, a group of linear variable differential transformers was used to evaluate vertical distribution of strain in the webs, and a curvemeter was used to verify slab curvatures indicated by the deck gages.

5. With the object in view of evaluating the validity of using distribution factors determined experimentally for this structure in the design of box girders with differing configurations of proportions, extensive analytical studies were conducted. Assuming that analytical methods could be derived which would accurately describe the empirically determined structural behavior of the prototype, such analytical methods could then be applied to other structures.

EXPERIMENTAL PROGRAM

Description of Field Prototype Structure

The structure chosen for testing was the Harrison Street Undercrossing, Bridge Number 33-289 OL, on Road IV-Alameda-5-Oakland (Fig. 1). The structure is part of the MacArthur Freeway, a major artery carrying traffic through the City of Oakland. Field tests were completed during the initial phases of construction of the freeway section in which the structure is located. A cross-section of the structure is shown in Figure 2.

The structure has one simple span of 80 ft, and rests on bearings which are normal to the centerline. Overall width is 34 ft, and width between barrier curbs and railings is 28 ft. There are five girder stems, inclosing four cells. Design was in accordance with the 1957 AASHO specifications. Design live loading was the H20-S16-44 and alternative loading.

After the structure had been chosen for testing, the following changes were made in the plans to conform to test requirements:

1. A rigid testing scaffold on timber piles just below the structure was added for support of the deflectometers.

2. Three-foot diameter holes were formed in the end diaphragms at the ends of each cell, and a gallery was added between each end diaphragm and the abutment backwalls.

Figure 1. Overall view of prototype test structure, showing deflectometer scaffold, instrumentation trailer inclosure, and test vehicle.

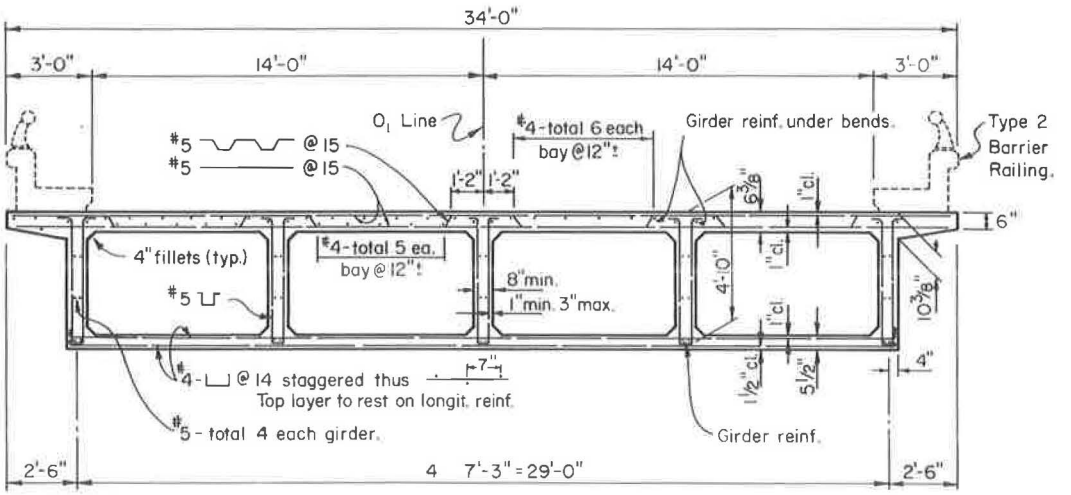

Figure 2. Cross-section of prototype test structure.

These features permitted access to the interior of the cells for removal of the forms from the soffit of the deck slab, for access to the gage installations, and for forming of the intermediate diaphragm.

3. Features were added to permit placement of the intermediate diaphragm after the deck slab was in place.

4. Blockouts, junction boxes, and gage installation were added.

With these exceptions, the plans remained unchanged, and the structure dimensions, reinforcement quantities, etc., were similar to what might be expected on any ordinary structure on the State highway system.

It is not standard procedure to remove the forms which support the deck slab within the cells, due to the inaccessibility of these forms after placing the slab. In this particular structure, these forms comprised plywood facing on closely spaced 2- by 6-in. beams resting on short posts supported on the bottom slab. Such support could be expected to contribute to the stiffness of the deck slab, and some question arose in the initial planning concerning the advisability of departing from the normal procedures in removing the forms; however, it is believed that under normal circumstances these forms will gradually deteriorate until the deck slab receives negligible support therefrom, and that removal of these forms would produce the worst, and most representative, condition for ultimate performance of the deck.

The manner of placing the intermediate diaphragm also represented a departure from normal procedures. This span length requires one diaphragm according to the 1957 and 1961 AASHO specifications, and it was felt that the test program would be enhanced by an attempt to evaluate the effects of inclusion of such a diaphragm on the distribution factors. Such an evaluation required that the structure be tested with and without this diaphragm. Ordinarily, of course, the intermediate diaphragm is placed monolithically with the stems and bottom slab. However, the intermediate diaphragm in this structure was placed after an initial series of crawl tests had been made without this structural component. Eight- and six-in. pipe nipples were placed in the deck slab above the diaphragm location (Fig. 3), and were closed at the tops by bar plugs, the lugs of which were placed about ½ in. below the riding surface of the deck slab to prevent interference with finishing or riding qualities. Three nipples were placed in the slab in each bay, the larger one in the center to be used for placement of the diaphragm concrete, and the two smaller ones at the outer limits of the bays to be used in venting the forms to prevent formation of air pockets.

After the first series of crawl tests had been completed without the intermediate diaphragm in place, the concrete above the nipples was removed with a chipping gun,

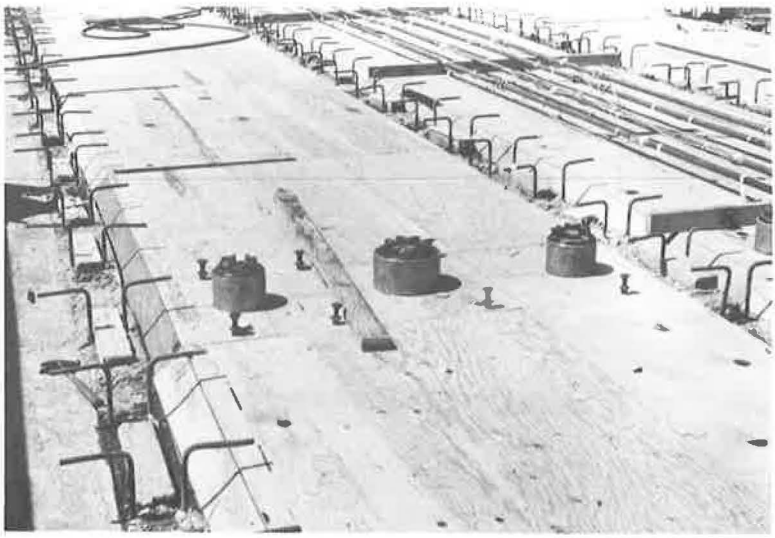

Figure 3. Pipe nipples placed in deck slab to permit interior diaphragm placement after first series of crawl tests.

Figure 4. Pouring intermediate diaphragm within cells of prototype structure between Phases II and III.

and the bar plugs were removed. Forms for the diaphragms were placed within the cells and braced by timbers bolted to inserts embedded in the slabs and webs around the peripheries of the diaphragms. Concrete was placed through the open nipples and carefully vibrated (Fig. 4). As was anticipated, considerable effort was required to vent the forms just below the deck slab and to obtain a tight fit; however, this effort was expended, the forms were carefully checked from within the cells during the pour, and a tight fit was obtained on all boundaries of the diaphragm.

Description of Instrumentation

Instrumentation placed in or on the superstructure, exclusive of the recording equipment placed in the instrument trailer (Figs. 5 and 6), fell into the following categories:

1. Carlson strainmeters were placed in the top slab at 30 locations, over the girder stems and at the midpoints of the bays. The axes of all gages were placed parallel to the structure centerline.
2. SR-4, AX-5, electrical resistance strain gages were placed on the main #11 reinforcing bars at the tops and bottoms of the girder stems and at the centerlines of bays in the bottom slab.

Figure 5. Exterior view of instrumentation trailer.

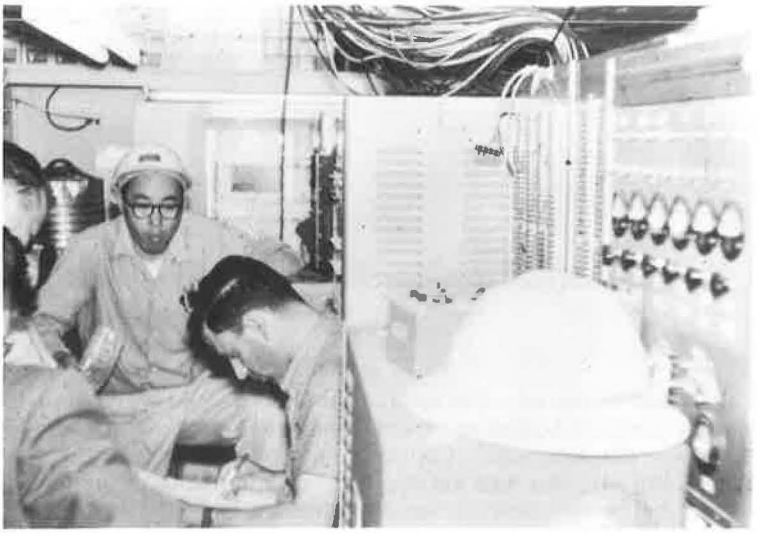

Figure 6. Interior view of instrumentation trailer with leads from 200 gages coming down through trailer ceiling.

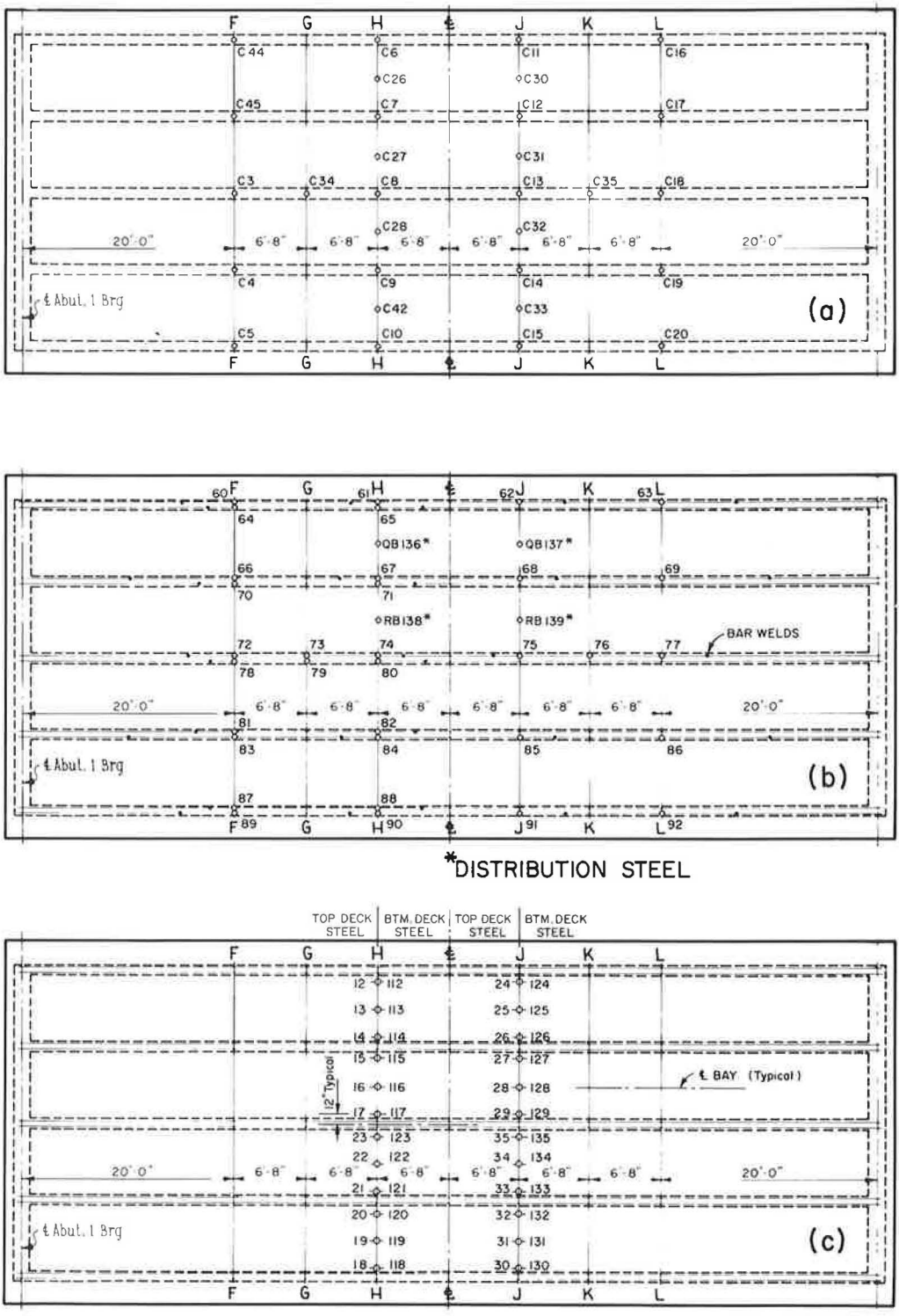

Figure 7. Prototype instrumentation: (a) Carlson strainmeters, top slab; (b) upper stem bars (#11) and distribution steel (#4); and (c) transverse gages, top slab.

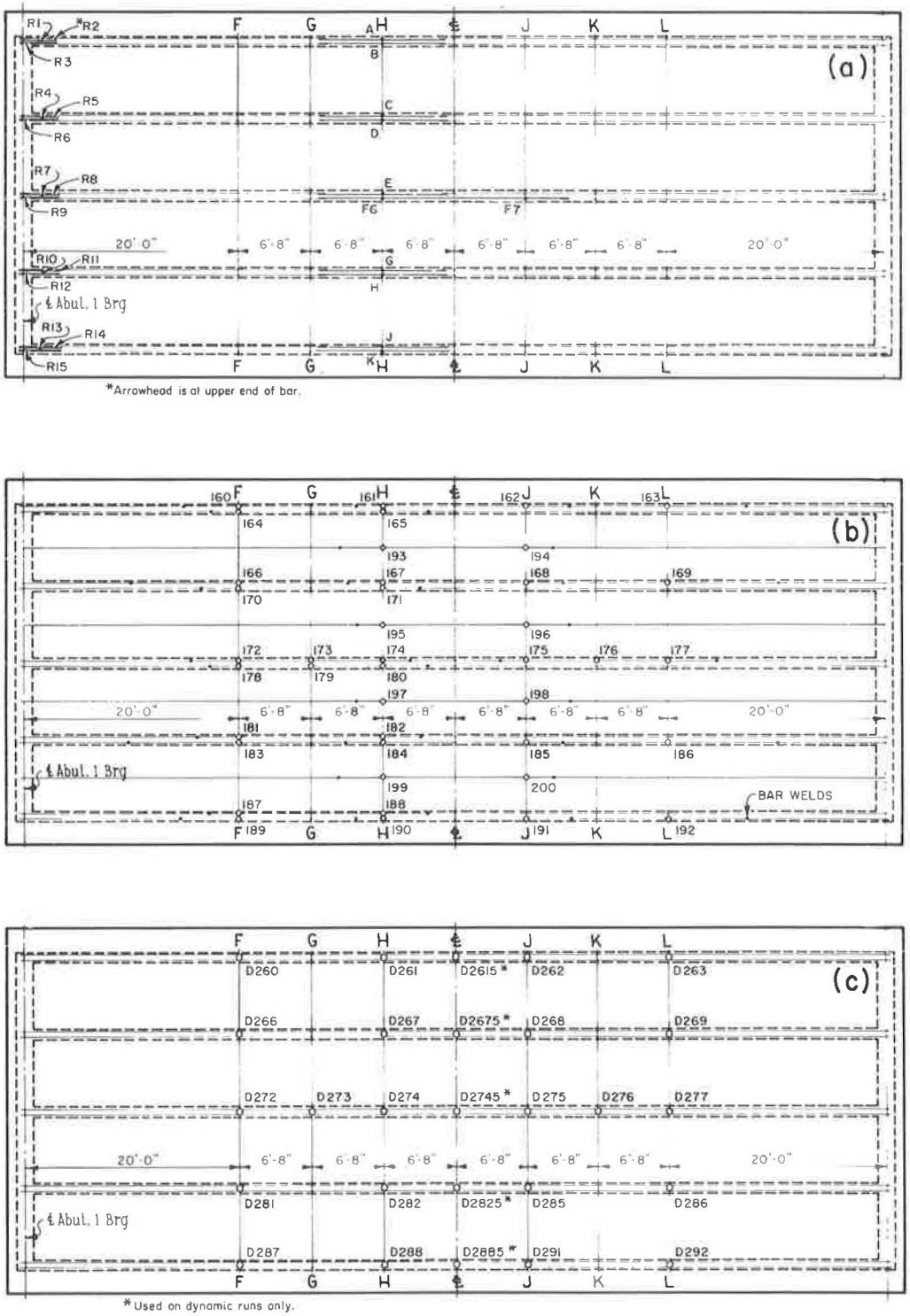

Figure 8. Prototype instrumentation: (a) lower third point bars (#5) and shear rosettes; (b) bottom slab reinforcement; and (c) deflectometer.

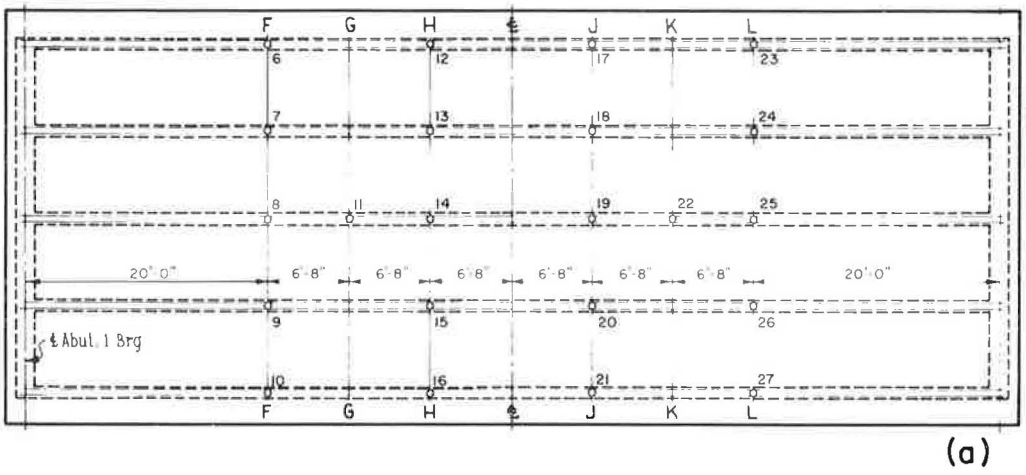

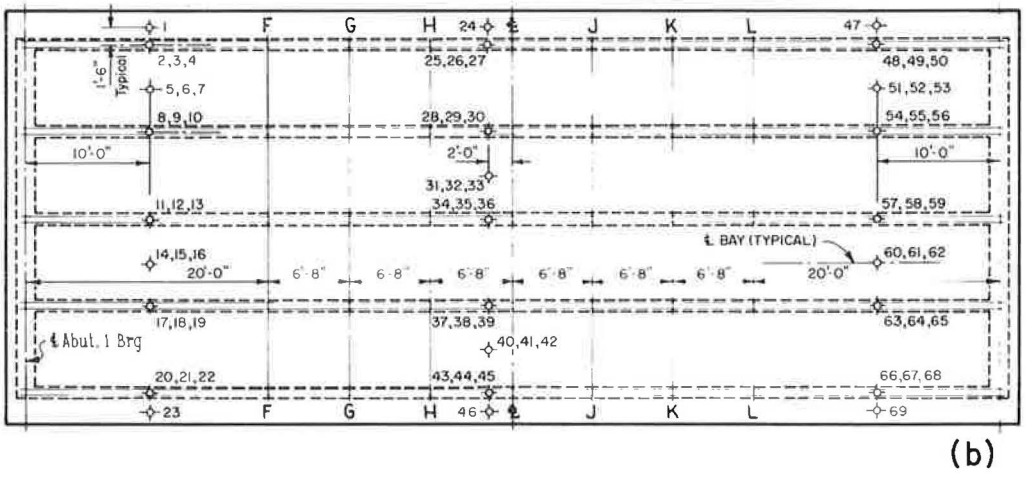

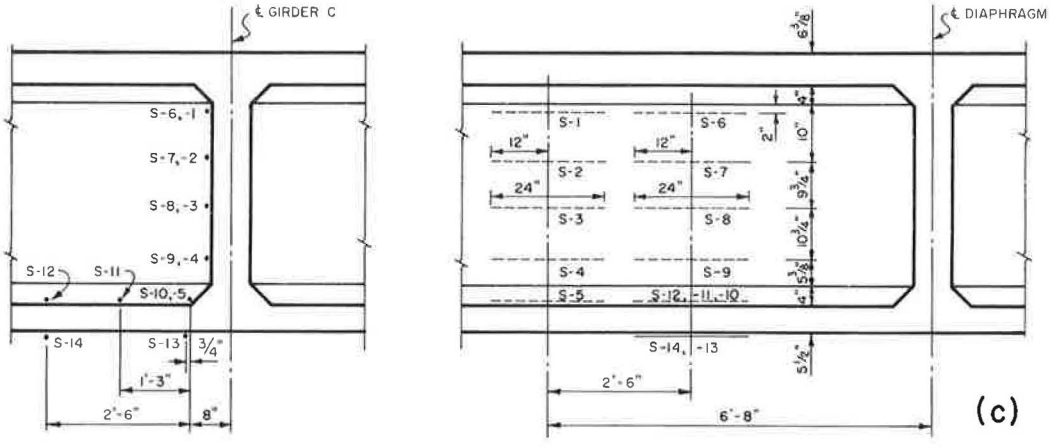

Figure 9. Prototype instrumentation: (a) copper bench nails; (b) thermocouples; and (c) LVDT locations.

3. SR-4, AX-7, electrical resistance strain gages were placed on the top and bottom transverse deck steel (#5 bars) over the edge of each fillet and at the centerlines of bays in two transverse sections.

4. At Abutment 1, a large shear rosette, comprising three gaged #5 bars, oriented at +45°, 0°, and -45° from the vertical, was placed in each of the five girder stems. Because the functional relationship of girder shear and skew is an unsolved problem, it was felt that the strain pattern in this area might prove valuable for latter comparison with other structures.

5. Deflectometers were placed on a rigid scaffold below the girders at 22 locations to permit measurement of live load deflections.

6. SR-4, AX-7, electrical resistance strain gages were placed on the #5 bars located in the stems 20 in. above the bottom slab soffit. The purpose of these gages was to determine the extent to which plane sections remained plane.

7. At four locations in the top slab, at the centerlines of bays, SR-4, AX-7, electrical resistance strain gages were placed on the longitudinal #4 distribution steel to measure local bending stresses in the deck slab in the longitudinal direction.

8. Thermocouples were placed at 69 locations in the superstructure to permit evaluation of internal temperature distribution.

9. Copper bench nails were placed at 32 locations in the deck surface for use in determination of dead load deflections of the superstructure by simple leveling methods.

10. A group of SR-4, A-9, electrical resistance gages and 12 inductance gages employing linear variable differential transformers were placed on one girder stem and at several locations on the bottom slab. These gages were added after it became evident that the gages at the lower third points of the stems were producing strain readings which were questionable.

11. Four "Tapeswitches" were placed on the riding surface to permit determination of longitudinal truck position.

Locations and numerical designations of the gages are shown in Figures 7, 8, and 9.

Because there were over 200 gages in the structure, and only 22 active recording channels on the oscillographs, it was necessary to group the gages in various combinations of 22 to be recorded simultaneously. A total of 28 combinations was established. An attempt was made to: (a) include every gage in at least one combination; (b) group the gages to produce simultaneous readings of the same types of stresses (e.g., girder shears, slab bending moments, longitudinal strains) at given transverse or longitudinal sections; and (c) provide sufficient overlap of gages from combination to combination to permit checks of reproducibility of strains.

Figure 10. Test vehicle traversing prototype structure at crawl speed; painted striping on deck to facilitate transverse positioning.

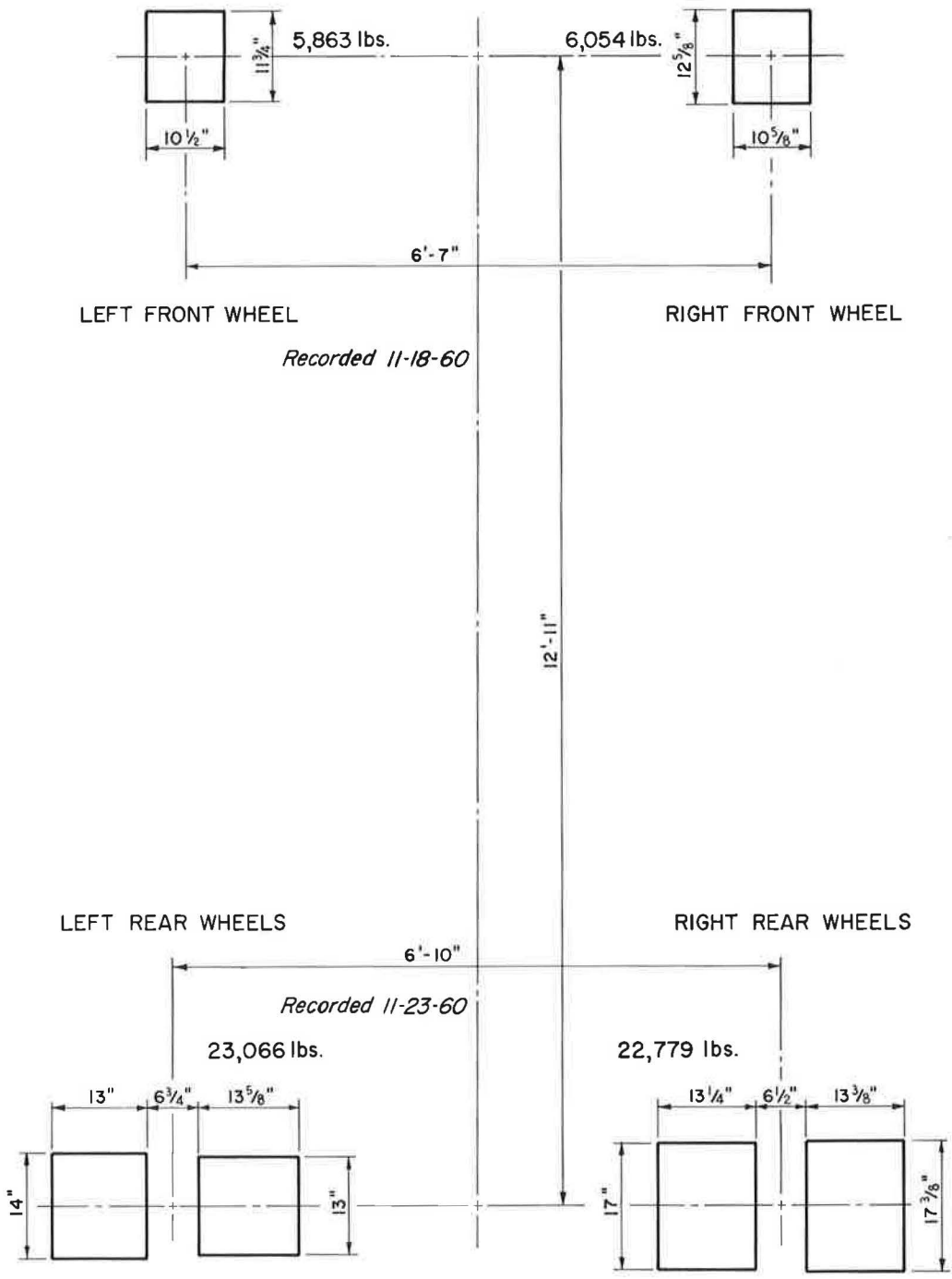

Figure 11. Dimensions and average, measured wheel reactions of test vehicle.

Figure 12. Typical measurement of test vehicle wheel reactions on Loadometer box.

Description of Test Vehicle

The vehicle employed in testing the structure was an R-15 rear dump Euclid truck loaded with steel ingots to a gross weight of 57 kips (Fig. 10). Pertinent dimensions and measured wheel reactions of the vehicle are shown in Figure 11, and a typical measurement of wheel reactions on the Loadometer box is shown in Figure 12.

Description of Materials Control Tests

Paralleling tests on the structure, tests were made to determine physical properties of the component materials used in its construction. Eighteen standard 6- by 12-in.

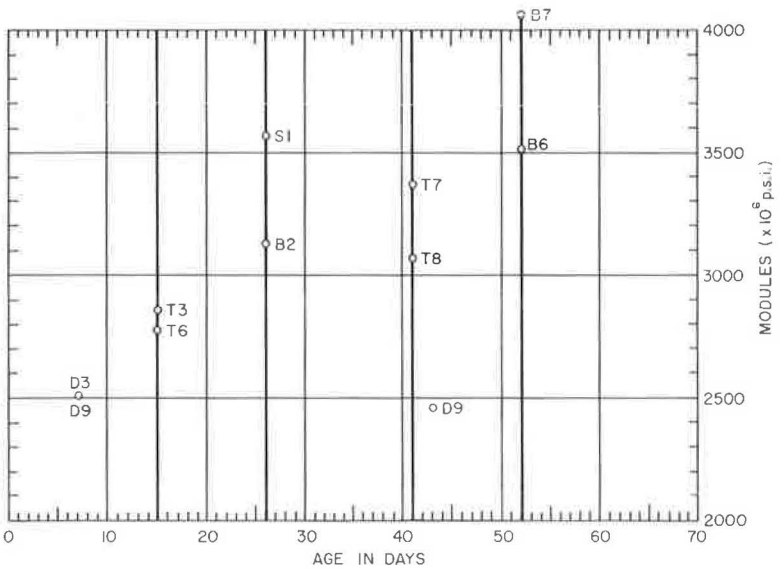

Figure 13. Axial concrete moduli based on 6-in. diameter by 12-in. cylinders.

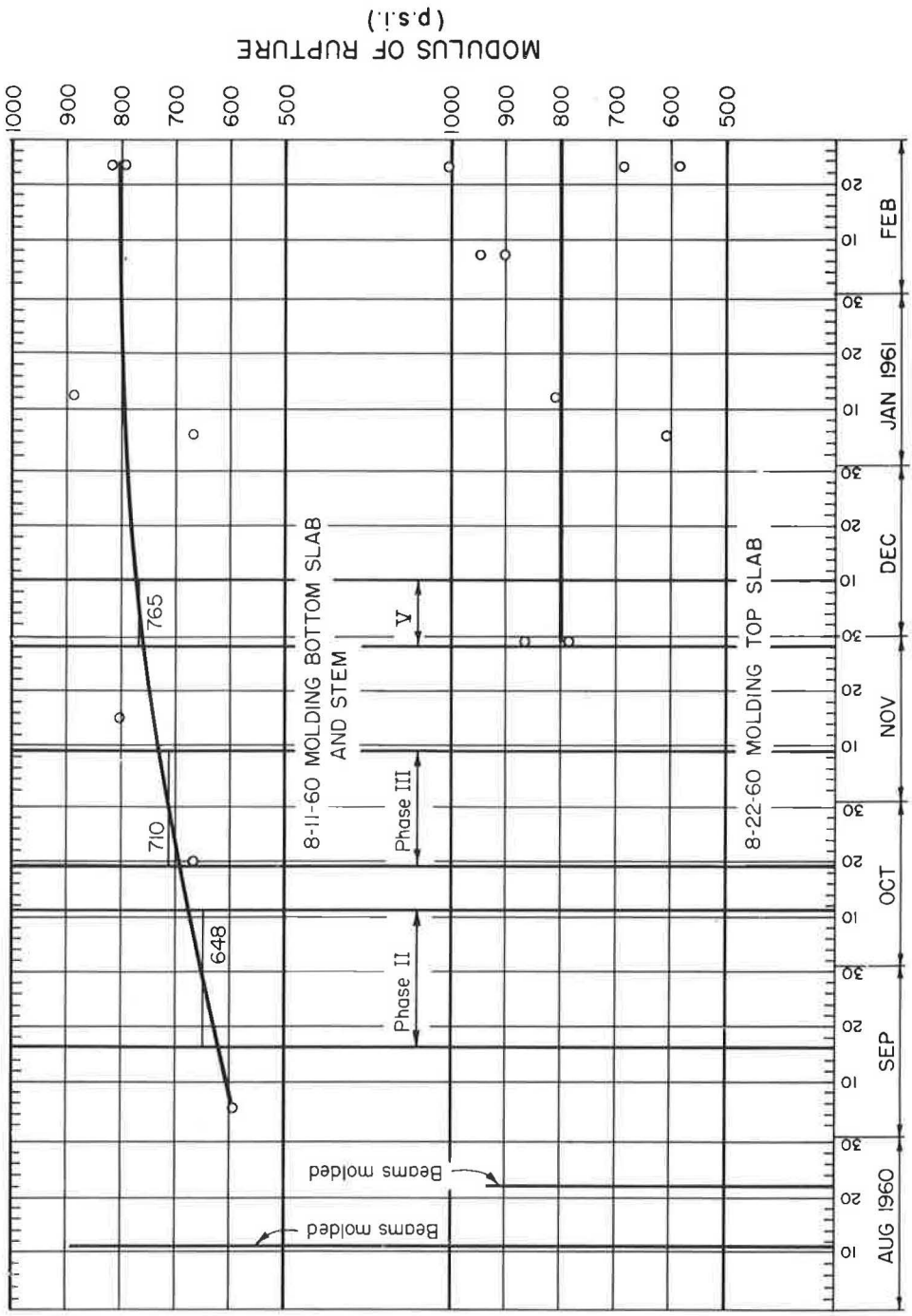

Figure 14. Modulus of rupture for prototype structure concrete.

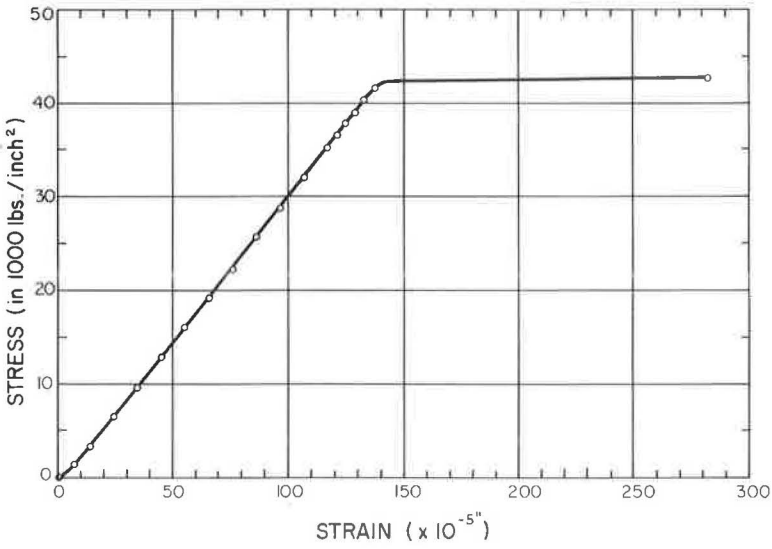

Figure 15. Typical stress-strain curve for #11 reinforcing bars placed in prototype structure.

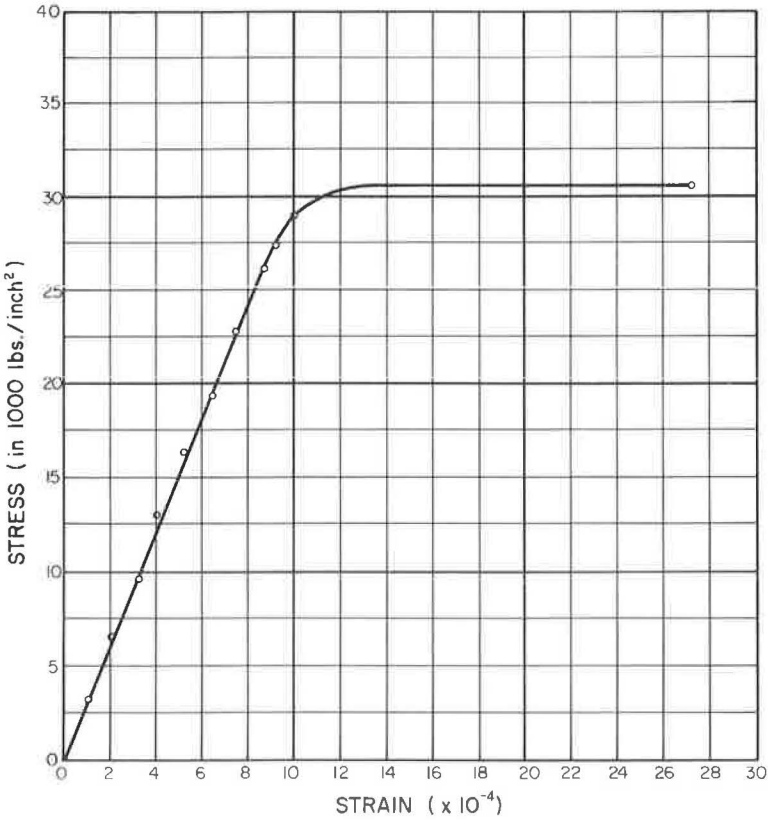

Figure 16. Typical stress-strain curve for #5 reinforcing bars placed in prototype structure.

Figure 17. Making measurements on one of the control test beams.

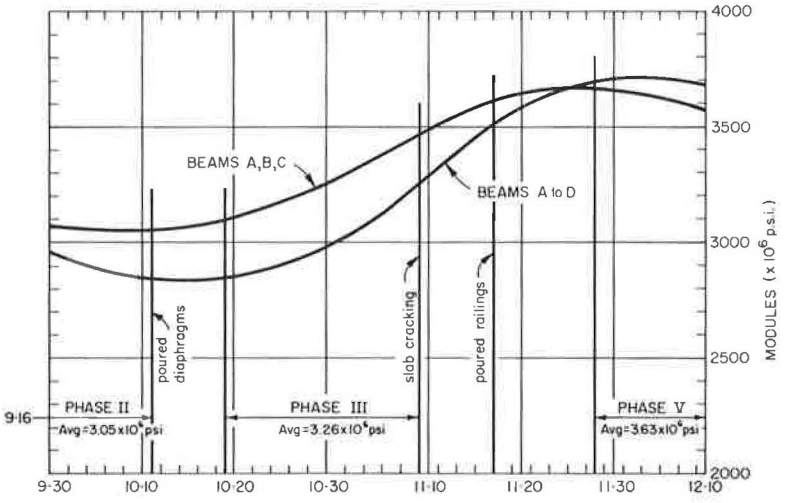

Figure 18. Axial moduli for prototype concrete based on measurements of control test beams.

diameter concrete cylinders were molded from each of the two main pours of the superstructure, four from the diaphragm pour, and seven from the barrier railing pour. Seven standard 6- by 6- by 34-in. modulus of rupture specimens were molded from the bottom slab and stem pour, and nine more from the top slab pour. Several tests were made of modulus of elasticity of the reinforcing steel used in the structure. Lastly, six $6\frac{3}{8}$- by 12-in. by 10-ft concrete control test beams were fabricated from batches chosen at random in the course of the deck pour.

Concrete Test Cylinders.—Test cylinders were fabricated in accordance with the instructions in the California Construction Manual. The specimens were kept in their metal molds under the structure until the time of testing when they were delivered to the University of California Engineering Materials Laboratory for determination of

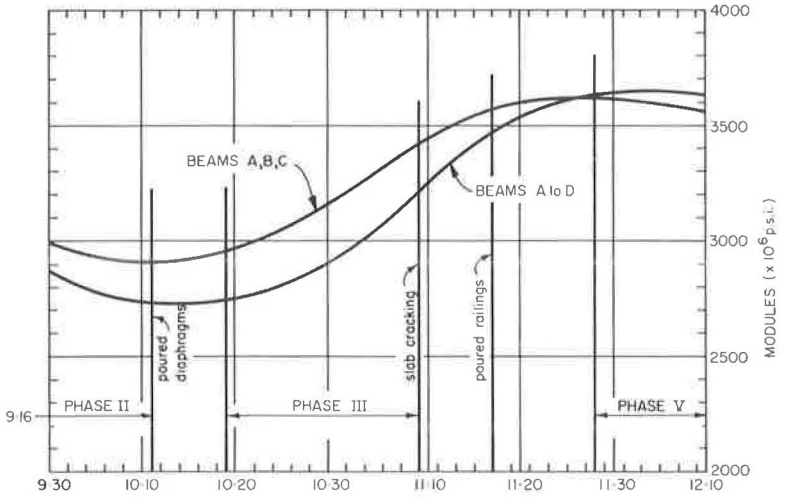

Figure 19. Bending moduli for prototype concrete based on measurements of control test beams.

elastic modulus, Poisson's ratio, and compressive strength. Measured values of modulus for the cylinders were erratic but are plotted in Figure 13.

Modulus of Rupture Specimens.—The 16 modulus of rupture specimens were fabricated in steel molds in accordance with instructions in the California Construction Manual. They were cured by burial in a pile of wet sand near the jobsite until they were broken in a three-point-loading beam-breaking machine. Plotted values of the modulus of rupture are shown in Figure 14.

Reinforcing Steel.—Figures 15 and 16 show stress-strain curves established by tests made by the Division of Highways Materials and Research Section for typical reinforcing bars chosen from the two primary sizes used in the structure. These curves were employed in the determination of the elastic moduli used in the data analysis.

Control Test Beams.—Four of the control test beams were tested on a continuing basis during the period the field prototype was being tested (Fig. 17). Final results of determinations of the elastic moduli of the concrete from these specimens are shown in Figures 18 and 19. The methods used to test the beams and derive these moduli are described in a final project report. The curves depict the mean values established from curves for three or four beams. The curves for Beam D were radically different from those of Beams A to C—it is believed this beam contained hairline cracks—so separate means were computed for Beams A to C and for all four beams.

Mean values of concrete modulus used in calculations for the three live load phases, taken from the three-beam curves of axial modulus, have been entered in Figure 18. Axial moduli differ from bending moduli because of marked variation of modulus through the slab depth. The axial modulus was used in resisting moment calculations because stresses of this type predominate in the top slab as a result of beam action.

EXPERIMENTAL RESULTS PERTINENT TO FIELD PROTOTYPE

The main portion of the research work pertinent to the prototype structure was divided into five phases, two of which were concerned with effects of live loads under varying conditions. In addition, slab stresses and deflections under wheel loads and very heavy concentrated loads were briefly studied, as well as the influence on the structure of heavy impact loadings. In all cases, interpretation of the data was complicated by pronounced departures from expectations based on idealized structural behavior and by the usual idiosyncracies of concrete behavior.

Dead Load Tests

Phase I was devoted to the study of deflections and bending strains under the influence of dead load of the bare box section and determination of the distribution of that load. During Phase IV, a similar study was made of the influence of the superimposed dead load of the barrier curbs and railings.

Each of these two phases entailed measurements, by simple leveling methods, of short- and long-term displacements of bench nails embedded in the deck slab over each stringer, as well as a continuing program of static measurement of internal strains.

Phase I Results.—Dead load deflection data were evaluated by plotting elevations of copper bench nails and computing displacements of each bench nail below the chords joining the abutment bench nails for the $\frac{1}{4}$-, $\frac{5}{12}$-, $\frac{7}{12}$-, and $\frac{3}{4}$-span points. Curves for the $\frac{5}{12}$ points of three girders are shown in Figure 20. "Instantaneous" values of dead load deflections were estimated by extrapolating the curves of best fit back to the time of striking falsework. Displacements obtained in this way are listed in Table 1. Values computed by theoretical methods described later in the report are tabulated for comparison.

To make distributions of bending strains more meaningful to the average designer, who is more familiar with specifications dealing with distributions of resisting moments, these moments were computed using stress components and moment arms based on the measured strains, employing the usual design assumptions for locating lateral limits of the stringers at midbays and edges of the deck slab. Computations of these resisting moments were subject to certain complications resulting from unanticipated anomalies in the strain measurements, coupled with the usual idiosyncrasies of concrete behavior. The former included: (a) the erratic distribution of dead load strains in the deck slab; (b) large, and obviously unrepresentative, temporary strains in the bottom slab reinforcement; and (c) larger discrepancies among stem and adjacent midbay strains than might reasonably be attributed to shear lag. The latter included the usual problems inherent in evaluating effects of creep, shrinkage, and cracking.

Twenty-four-hour strains for 16 midbay gages are listed in Table 2. The strains listed in each quadruplet were measured by gages located at the corners of a rectangle whose axes of symmetry coincided with those of the structure. Under the influence of the symmetrical dead load, the four readings might reasonably be expected to be the same. The erratic strain distribution which actually was manifested in the top slab readings probably resulted from variations in concrete modulus. Although a slump tolerance of $\pm 1\frac{1}{2}$ in. was maintained in superstructure construction, measurements for the control beams evidenced the fact that large variations in concrete modulus were possible; indeed, measured moduli varying by factors as great as $2\frac{1}{2}$ across the $6\frac{3}{8}$-in. beam depth were common. Such variations might result from different curing rates at top and bottom, nonhomogeneity and segregation of the vibrated mass, or differential shrinkage cracking.

Despite the possible existence of local "hard" and "soft" spots in the deck slab, it may be expected, because of the stiffness of the end diaphragms, that the longitudinal strains averaged over the entire span would be equal for symmetrically located cells. Although the determination of such average values would require knowledge of the entire longitudinal strain distribution, an insufficiency of gages precluded this; however, longitudinal averaging of strains measured at the $\frac{5}{12}$ and $\frac{7}{12}$ points produced marked transverse strain symmetry (Table 3). It may be argued, of course, that averaging for two sections does not necessarily produce a representative average.

Similar longitudinal averaging of bottom slab reinforcement strains measured 24 hr after striking falsework did not produce similar transverse symmetry. Compilations of strains at later periods, however, demonstrated that transverse symmetry was markedly improved after 24 hr (Table 4). This observation led to the plotting of strain-time curves for these bottom slab gages. These curves demonstrated that, after the initial 24-hr readings, the bottom slab reinforcement strains remained essentially constant with time; however, in general, the 24-hr strains differed radically from the ordinates of the curves extrapolated back to this time. Extrapolated strain values are also listed in Table 4.

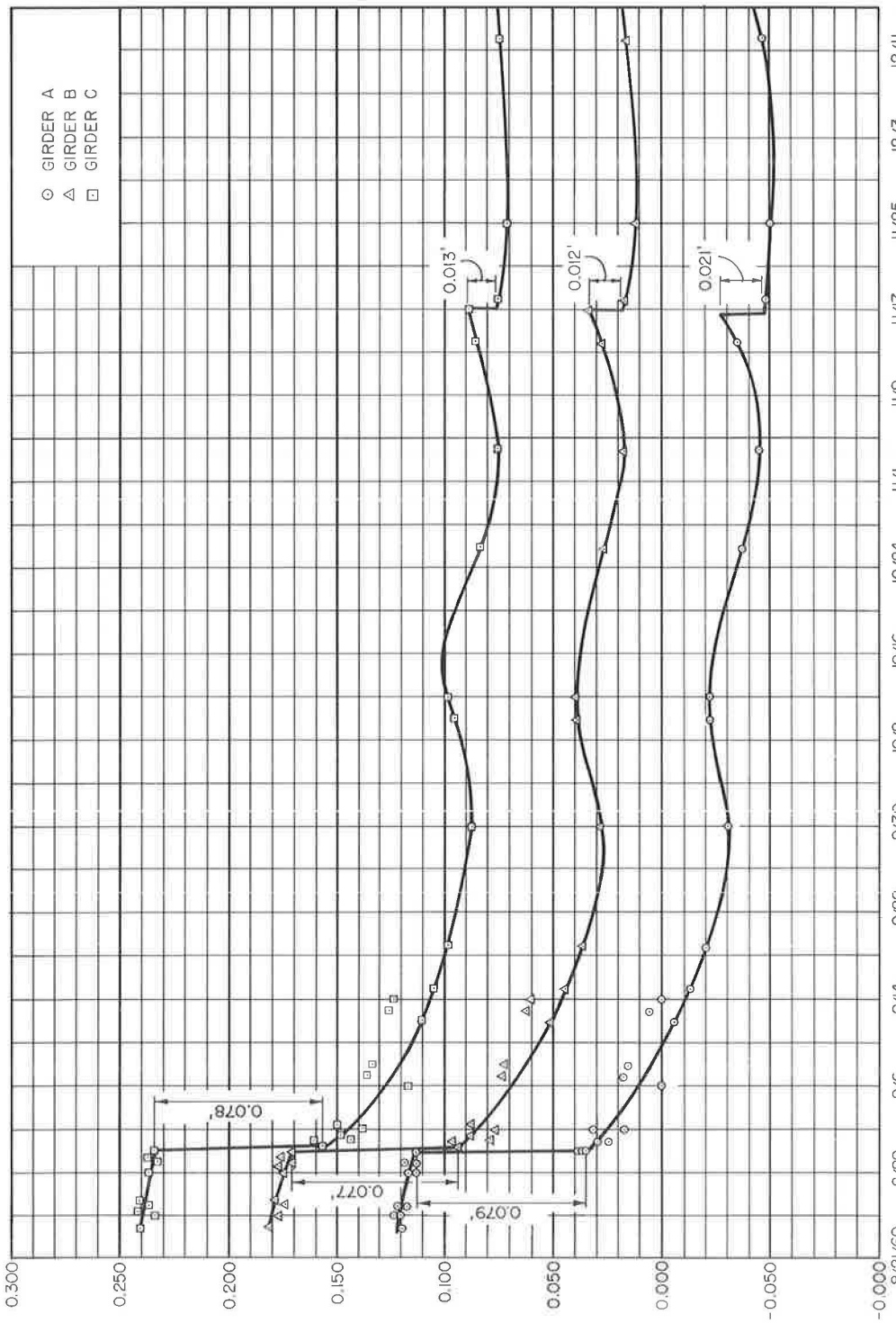

Figure 20. Dead load deflections of stringers A, B, and C, at 5/12 point of span taken from levels on copper bench nails embedded in deck.

TABLE 1

DEAD LOAD DEFLECTIONS

Girder	Deflection	
	Exper.[a] (ft)	Theor. (ft)
A	0.079	0.077
B	0.077	0.077
C	0.078	0.077
D	0.075	0.077
E	0.080	0.077

[a]Average of deflections 5/12 and 7/12 points.

TABLE 2

24-HOUR STRAINS FOR 16 MIDBAY GAGES

Gage	Strain (μ in./in.)	Gage	Strain (μ in./in.)
(a) Top Slab			
C26	-460	C27	-555
C30	-306	C31	-285
C42	-546	C28	-310
C33	-251	C32	-472
(b) Bottom Slab			
193	641	195	499
194	456	196	597
199	438	197	327
200	334	198	563

Large differences among stem and midbay strains necessitated assumption of a distribution pattern in the intervening slab area; a parabolic distribution was assumed.

An explicit evaluation of the effects of creep and shrinkage would have been very difficult for this field test. Existence of pronounced creep strains was evident from the deflection-time and deck slab strain-time curves, although little or no evidence existed for any influence of creep on the lower slab reinforcement strains. It is hypothesized that the creep strains were augmented by the closing of transverse cracks in the deck slab resulting from differential shrinkage of the deck slab against the restraint of the lower slab and stem section. The stems and lower slab were poured monolithically, and the deck slab was poured 11 days later.

Although an explicit determination of the effects of creep and shrinkage would be difficult, these effects may be accounted for implicitly in dead load moment calculations by one of two methods:

1. The strain pattern in the deck slab and stems may be used to determine the location of the resultant compressive total stress and moments due to total tensile stresses in the reinforcing steel computed about this location; or
2. An "effective" concrete modulus may be determined such that the total compressive stress, determined from this modulus and the measured strain distribution, is equal to the total tensile stress, and moments produced by the two types of stress may be computed about the experimentally determined neutral axis; moments due to total stresses in compressive reinforcement are, of course, computed explicitly.

After the aforementioned longitudinal averaging of strains for the $^5/_{12}$ and $^7/_{12}$ points, the resultant strains were also averaged transversely. The final strain distributions used in determination of dead load moments based on strains read at 24 hr and 15 days after striking falsework are shown in Figures 21 and 22, respectively. Resisting moments, total stresses, and the "effective" concrete moduli required to balance total stresses across the transverse section are shown in Table 5. Table 6 lists the moments due to the panel loads computed in accordance with 1961 AASHO specifications; these computed moments include the couples due to flared transitions in the ends of the stems. Table 7 lists dead load moments distributed to each stringer as computed by a theoretical method discussed later in this report.

The figures in the tables evidence the fact that, when values of concrete modulus compatible with static balance of total stresses across the transverse section were used in determination of resisting moments (moments computed implicitly in terms of reinforcing steel total stresses were essentially the same), the total section moments determined empirically agreed very closely with the total of computed dead load panel

TABLE 3

TOP SLAB STRAINS PRODUCED BY FALSEWORK REMOVAL

Location	Gage	9-1-60				9-15-60			
		Indicated Strain	I. S.[a] / 2.462	Mean	Mean	Indicated Strain	I. S.[a] / 2.462	Mean	Mean
Girder A	61	-				-1,268	-525		
H-H	C 6	-325				- 546		-553	
	65	-863	-358	-342		-1,419	-588		
					-304				-522
J-J	62	-700	-290			-1,198	-497		
	C11	-241		-266		- 456		-477	
Bay A-B:									
H-H	C26	-460				- 699			-577
J-J	C30	-306			-383	- 455			
Girder B	67	-815	-337			-1,356	-561		
H-H	C 7	-350				- 565			
	71	-920	-380	-356		-1,450	-600	-575	
					-377				-613
J-J	68	-920	-380			-1,532	-634		
	C12	-440		-410		- 706		-670	
Bay B-C:									
H-H	C27	-555				- 802			
J-J	C31	-285			-420	- 519			-661
Girder C	74	-940	-388			-1,459	-602		
H-H	C 8	-401				- 643			
	80	-880	-363	-384		-1,408	-581	-609	
					-359				-581
J-J	75	-770	-319			-1,342	-555		
	C13	-324		-322		- 524		-540	
Bay C-D:									
H-H	C28	-310				- 484			
J-J	C32	-472			-391	- 733			-609
Girder D	82	-815	-334			-1,374	-564		
H-H	C 9	-306				- 531			
	84	-800	-328	-323		-1,355	-556	-550	
					-330				-555
J-J	C14	-345				- 574			
	85	-815	-335	-340		-1,340	-550	-562	
Bay D-E:									
H-H	C42	-546				- 809			
J-J	C33	-251			-399	- 470			-640
Girder E	88	-915	-375			-1,416	-581		
H-H	C10	-350				- 556			
	90	-820	-336	-354		-1,330	-546	-561	
					-328				-535
J-J	C15	-302				- 509			
	91	-670	-275	-289		-1,179	-484	-497	

[a]Corrected for lead length resistance; lead length correction equal to $1 + 2RL/R_{SR4}$, and applies only to SR4 gages.

TABLE 4

BOTTOM SLAB STRAINS PRODUCED BY FALSEWORK REMOVAL

Location	Gage	9-1-60[a]				9-15-60[c]				9-1-60[b]		
		Indicated Strain	I.S.[c]/2.462	Mean	Mean	Indicated Strain	I.S.[c]/2.462	Mean	Mean	I.S.[c]/2.462	Mean	Mean
Girder A	161	1,150	476			1,179	488			465		
H-H	165	1,155	478	477		1,245	515	502		473	469	
					461				482			455
J-J	162	1,035	429	429		1,068	442	442		428	428	
Bay A-B:												
H-H	193	1,550	641			1,010	418			410		
J-J	194	1,100	456		549	900	373		396	372		391
Girder B	167	1,290	532			1,330	549			535		
H-H	171	1,095	452	492		1,290	532	541		519	527	
					489				526			513
J-J	168	1,170	484	484		1,200	496	496		484	484	
Bay B-C:												
H-H	195	1,210	499			950	392			371		
J-J	196	1,445	597		548	890	368		380	357		364
Girder C	174	1,398	575			1,353	557			551		
H-H	180	1,385	570	573		1,320	543	550		553	542	
					540				525			516
J-J	175	1,150	475	475		1,150	475	475		465	465	
Bay C-D:												
H-H	197	795	327			890	366			366		
J-J	198	1,365	563		445	885	365		366	351		359
Girder D	182	1,260	518			1,245	512			492		
H-H	184	1,350	555	537		1,250	514	513		504	498	
					538				506			488
J-J	185	1,310	540	540		1,190	491	491		467	467	
Bay D-E:												
H-H	199	1,065	438			945	388			366		
J-J	200	810	334		386	860	355		372	334		350
Girder E	188	1,080	443			1,260	517			479		
H-H	190	1,180	484	464		1,100	451	484		464	471	
					479				470			461
J-J	191	1,240	511	511		1,075	443	443		426	426	

[a]Strains shown are actual differences between strains read just before striking false work and those read about 24 hr later, and those read 15 days later.
[b]Strains obtained by graphical extrapolation of best smooth curve drawn visually through strain reading from 8-31 through 10-10-60, in general disregarding first 24-hr reading.
[c]Readings corrected for lead length resistances.

moments. Moreover, the distribution factors for individual stringers agreed very favorably with factors computed on the basis of folded plate theory.

Inasmuch as the value of "effective" concrete modulus required to produce static balance is quite low compared with the 9-day cylinder test value of 2,600,000 psi, an attempt was made to evaluate possible relative magnitudes of creep and shrinkage. By assuming that any transverse cracks due to differential shrinkage would close immediately on striking falsework, after which combined creep and shrinkage occur, it is possible to establish a rough approximation of the magnitude of initial cracking by establishing an approximate value of instantaneous strain.

Figure 23 illustrates three typical plots of the strain-time relationship for deck slab gages. Curve-fitting methods were used to determine equations comparable to the following equation established by Billig (1) for the creep strain-time relationship in unreinforced concrete:

$$e_t = (1 + \phi_t)\ c/E_o \qquad (1)$$

where

e_t = strain due to creep,
$\phi_t = 1.26\ (t)^{1/3}$,

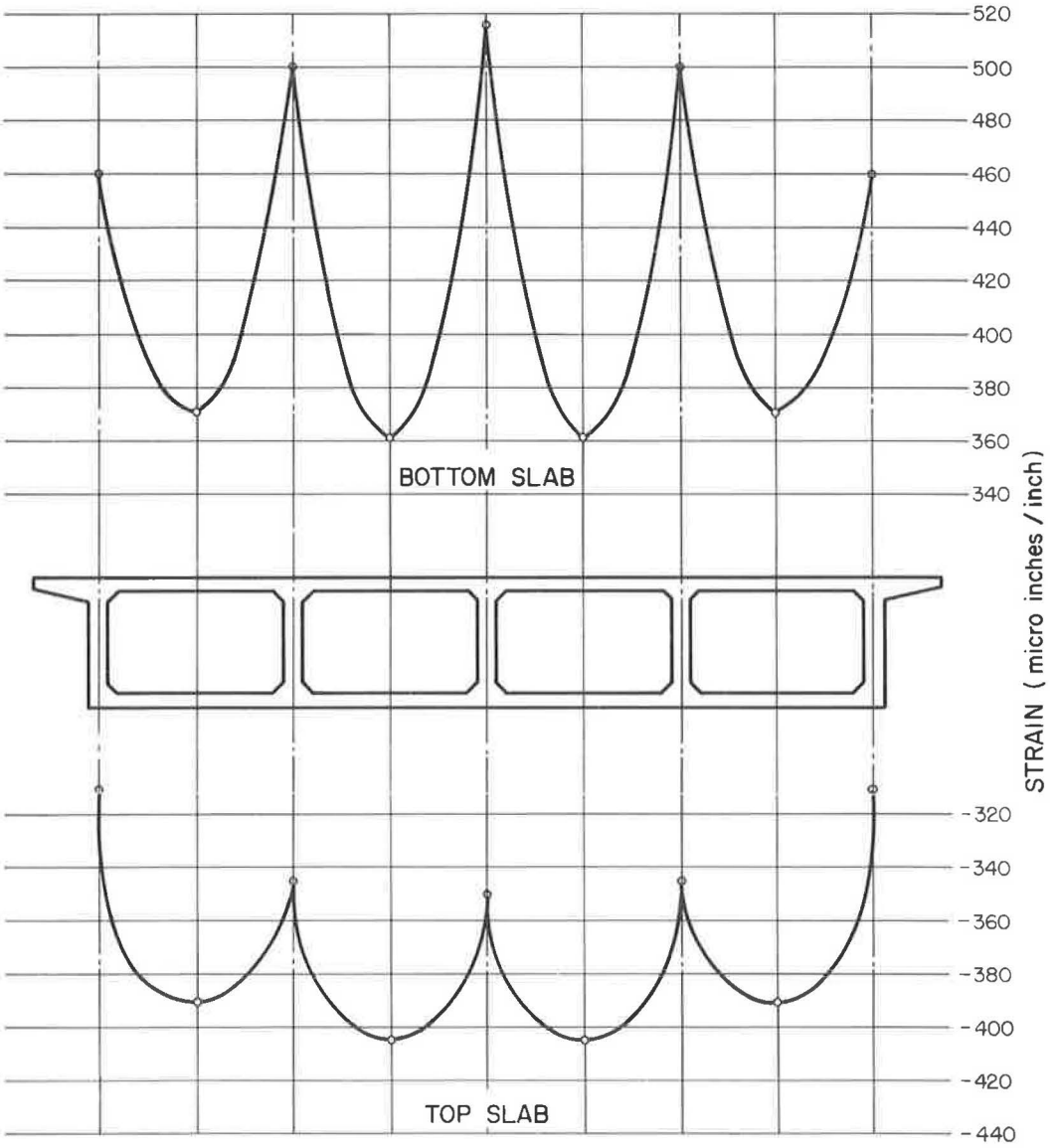

Figure 21. Assumed average distribution of dead load strains 24 hr after striking falsework.

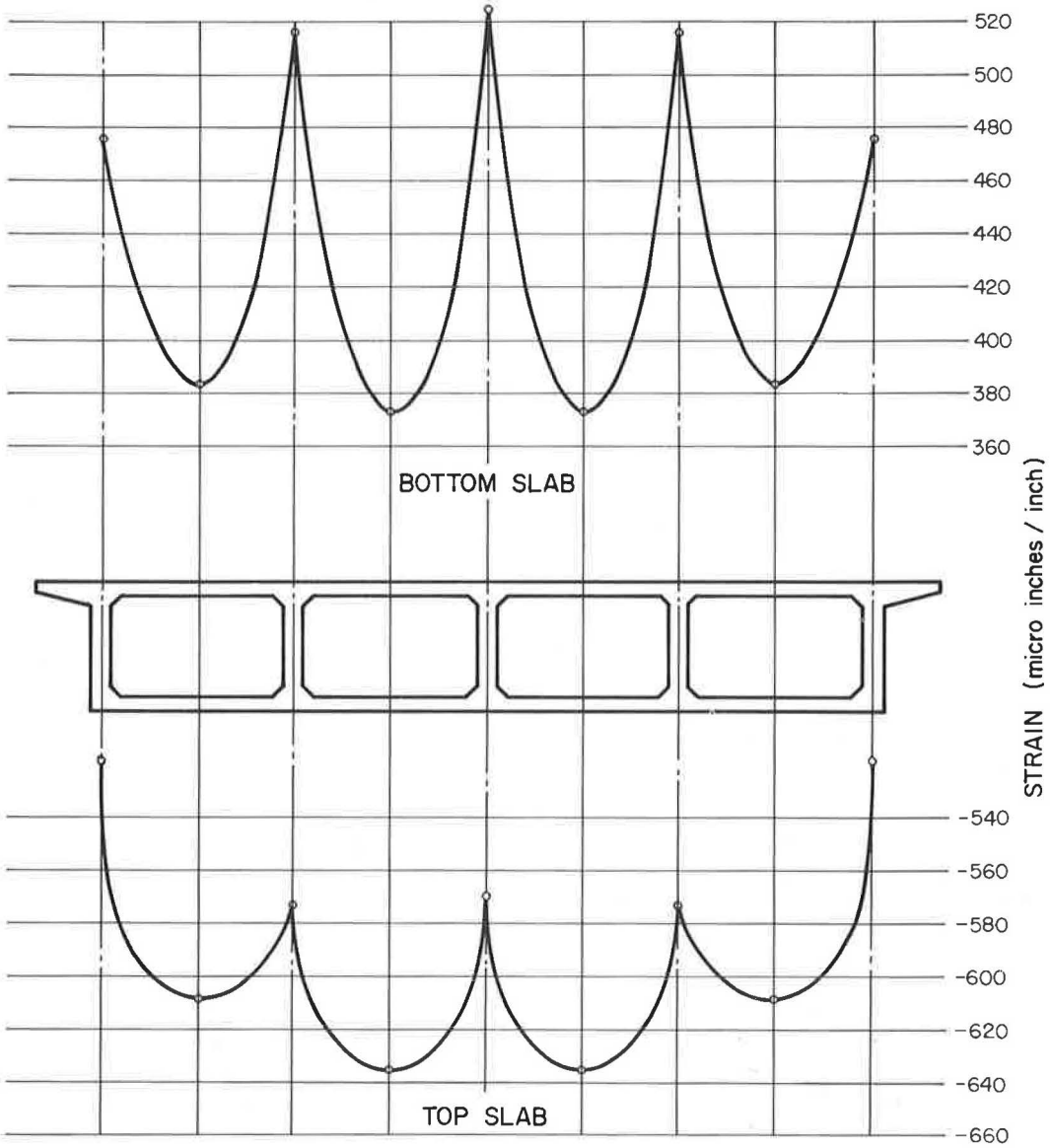

Figure 22. Assumed average distribution of dead load strains 15 days after striking falsework.

TABLE 5

COMPUTED DEAD LOAD MOMENTS AND TOTAL STRESSES

Time	E_c (ksi)	Girder	Moment (kip-ft)	Percent Total	Compressive Total Stress (kips)	Tensile Total Stress (kips)
24-hr	954.9	A, E	870	16.0	242	197
		B, D	1,231	22.6	277	296
		C	1,248	22.9	283	299
Total[a]			5,450	-	1,285	1,285
15-day	495.1	A, E	913	16.4	235	203
		B, D	1,245	22.4	283	305
		C	1,254	22.5	286	305
Total			5,570	-	1,322	1,321

[a]Five girders.

t = time after loading (mo),
c = stress, and
E_o = design modulus of elasticity.

Although this particular equation could not be expected to hold for reinforced concrete, it was found that an equation of the same general form with different constants,

$$e_t = c(1 + kt^a) \quad (2)$$

produced curves conforming closely to the measured data. It has been assumed that if suitably chosen values of c, k, and a produced curves which closely approximated the empirical data, the values of c would approximate the instantaneous strain, free of creep. Using values taken from such curves, the ratios of instantaneous to 24-hr strains are listed in Table 8. The instantaneous strains average about 75 percent of the 24-hr strains.

The ratio (955,000/2,600,000) of modulus computed for static balance to the 9-day cylinder test value requires a reduction of strains to 37 percent of their 24-hr values for determination of instantaneous strain. The 24-hr strain would then comprise the following: (a) 90 μ in. of creep strain; (b) 37 percent of 365, or 135 μ in. of dead load strain; and (c) 140 μ in. of shrinkage crack closing. The latter figure compares

TABLE 6

DEAD LOAD MOMENTS COMPUTED ON BASIS OF 1961 AASHO SPECIFICATIONS

Girder	Moment (kip-ft)	Percent Total Moment
A, E	945	17.5
B, D	1,169	21.7
C	1,169	21.7
Total[a]	5,397	-

[a]Five girders.

TABLE 7

THEORETICAL DEAD LOAD MOMENTS (Third Method)

Girder	Moment (kip-ft)	Percent Total Moment
A, E	846	0.158
B, D	1,218	0.228
C	1,215	0.227
Section total	5,343	-

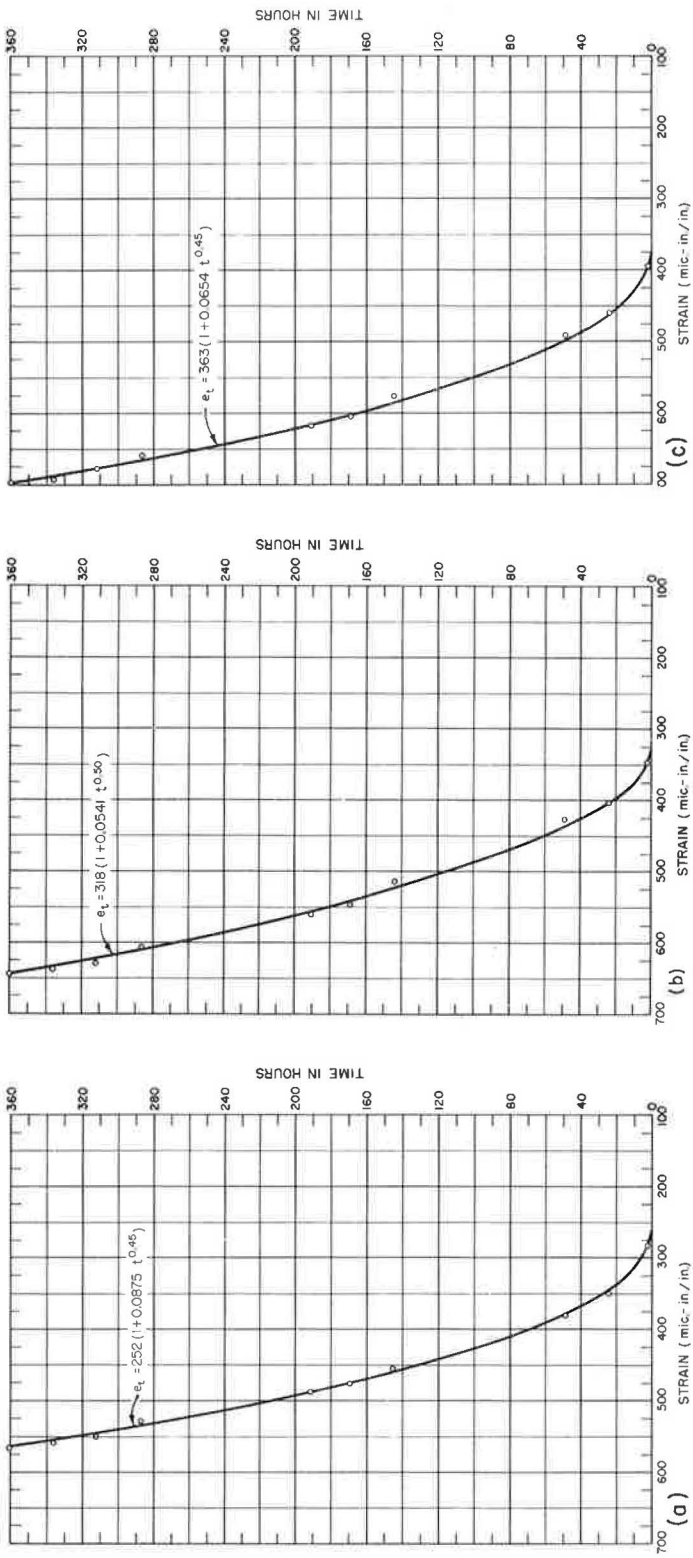

Figure 23. Typical dead load strains in top slab as functions of time using Carlson strainmeters: (a) C7, (b) C8, and (c) C26.

TABLE 8

RATIOS OF COMPUTED INSTANTANEOUS TO MEASURED 24-HOUR STRAINS

Gage	Strain (μ in./in.)		Ratio (%)
	Est. Instantaneous	24-Hr[a]	
C 6	230	322	71.4
C 7	252	344	73.3
C 8	318	403	78.9
C 9	227	305	74.4
C10	251	354	70.9
C26	363	463	78.4
Avg	274	365	74.6

[a]From curve.

favorably with the usual shrinkage coefficient of 0.0002 (200 μ in./in.) and with a measured shrinkage of 110 μ in. in Control Beam C between the ages of 16 and 29 days and about the same amount for Beam A between ages of 16 and 39 days.

Phase IV Results.—Strains measured during the application of the superimposed dead load of barrier curbs and railings were small and too erratic to be of value in determination of induced resisting moments.

Live Load Tests

Phases II, III, and V entailed evaluation of influences on deflections and internal bending strains of a heavily loaded test vehicle moving across the span at crawl speeds of 2 to 5 mph. Strains and deflections measured by internal gages and deflectometers were recorded on oscillographic equipment housed in the instrumentation trailer parked beneath the structure. Frequent static readings were taken with the test vehicle on the span to permit checking of calibration procedures. The resulting correlations were excellent; however, the dynamic loading methods were superior to the static methods for two reasons: (a) the intervals between loading and unloading were shorter and strain variations due to temperature changes were negligible; and (b) very large variations in the patterns of general bending strains, which result from local effects of wheel loads, could readily be evaluated or eliminated by smoothing the oscillographic traces. At the low speeds employed, dynamic effects on the strain patterns were negligible.

Phase II was devoted to the study of structural action of the bare box section. Between Phases II and III, a single intermediate diaphragm was placed within the structure at midspan to permit evaluating the influence during Phase III of such a diaphragm on structural behavior. Between Phases III and V, barrier curbs and railings were placed on the structure, and crawl testing was continued during Phase V to determine the extent to which strains and deflections were modified by these structural components.

Comparison of results based on test data obtained using only one test vehicle with stringer moments based on specifications which permit two vehicles to occupy the span required assumption of validity of the principle of superposition. Crawl tests were performed with the test vehicle occupying 12 transverse positions on the deck slab (Fig. 24), and longitudinal strains were plotted as functions of transverse position. The resulting curves were averaged graphically for symmetrically placed gages for symmetrical test vehicle positions; the symmetry of these strains was very marked, the variation of one curve from its symmetrical counterpart seldom exceeding 2 μ in./in. Strains for four hypothetical vehicle positions were established from the resulting average curves and superposed in the following two vehicle position combinations. (Position 4.10 denotes that the left rear dual wheel is centered at 0.10 of the distance between Positions 4 and 5 from Position 4; Position 11.43, that the right rear dual is located 0.43 of the distance between Positions 11 and 12 from Position 11.) Vehicles were assumed to be confined to separate lanes as in the specifications:

1. Position 4.10 + 11.43—critical loading for center girder;
2. Position 4.10 + 11.93—critical loading for first interior girder; and
3. Position 4.10 + 12.30—critical loading for exterior girder.

As in the case of dead load testing, data analysis was complicated by certain departures from idealized structural behavior. Chief difficulties were as follows:

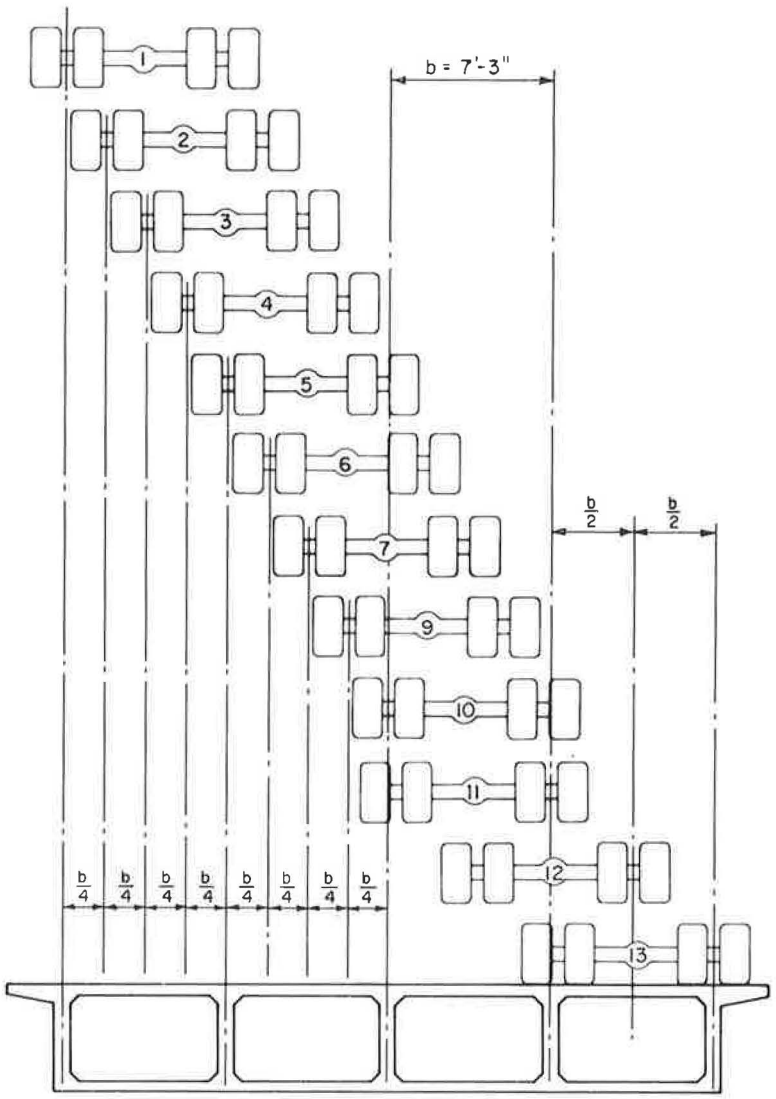

Figure 24. Transverse positions of test vehicle used in live loading of prototype structure.

1. Larger discrepancies among stem and midbay strains existed than those anticipated from shear lag considerations, necessitating assumption of a pattern of strain distribution in the intervening bars and slab sections; again a parabolic distribution was assumed between each midbay strain and the adjacent stem strain, the former being at the parabola's vertex.

2. Simultaneous satisfaction of statics was lacking for total stresses and total resisting moments across given transverse sections of the structure. The total compressive stresses, computed from the measured strain patterns and the concrete moduli determined for the control test beams, invariably exceeded the total tensile stresses computed from the measured steel strains and calibration factors established in the laboratory for total bar stresses as functions of measured strains, and from measured steel moduli. Arbitrary reduction of concrete moduli to effect static balance of total stresses only increased a large discrepancy between external and internal moments.

3. There was lack of agreement between the total internal resisting moments, computed from known concrete and reinforcement properties and measured strains, and the external moments which can be computed from known loads and positions of the test vehicle.

Depending on the manner in which empirical data from live load tests are treated in the computation of girder resisting moments, the discrepancies between summations of those moments for the five stringers and the external moments known to be acting on the structure due to the test vehicle can reach magnitudes as great as 30 percent or as little as 2 percent, the external moment exceeding the internal.

This latter departure from idealized structural behavior appears not to be unique to this particular study; it has probably occurred more frequently than published test results would indicate. Several possible contributing factors have been examined. Tests performed in 1958 by the University of Iowa (2) on a continuous, composite, steel girder bridge evidenced a 23 percent discrepancy between known external and measured internal resisting moments. In the authors' discussion of this discrepancy, the major portion (20 percent) was attributed to distributing effects of the concrete slab; that is, a concentrated wheel load was assumed to act as such on the girder over which it was placed, but, due to the presence of the concrete slab, as a distributed load on girders removed therefrom, resulting in a reduction of computed total resisting moment. Although this explanation has its appeal, it is believed that satisfaction of the principles of static equilibrium across a given transverse section demands that moments in the comparatively flexible slabs (the top slab stiffness being roughly 0.4 percent of the summation of girder stiffnesses) would have to contribute the deficient portion of the total moment.

The second possibility which suggests itself depends on the existence of possible tensile stresses in the concrete below the neutral axis. The resisting moments were computed for cracked sections. In connection with this argument, the following points should be considered:

1. Visible evidence existed, on stem faces, of cracking almost to the computed level of the neutral axis for the cracked section; moreover, the measured strains at tops and bottoms of stems verified these locations.
2. Computed total resisting moments for the gross section are much greater than the external moments. However, if the stems are assumed to remain uncracked down to the top of the lower slab, the computed resisting moment becomes nearly equal to the external moment. In this event, however, the total computed tensile stress becomes much greater than the total computed compressive stress. Also, with live load strains of roughly 60 μ in./in. combined with dead load strains of 450 μ in./in. at this upper limit of cracking, the concrete would be sustaining tensile stresses of about 1,550 psi. Using the usual assumption that tensile strength is about half the modulus of rupture, the limiting tensile strength should be about 400 psi.

As a third possibility, the measured strains in the gaged bars may not accurately represent those in the intervening bars. At each gage location, a blockout was cast into the concrete to permit gage replacement. If it may be logically assumed that the longitudinal strain distribution in a reinforcing bar is nonuniform, exhibiting maxima at the cracks and minima midway between cracks where tensile stress in the concrete participates in carrying load, then the average strain measured in a blocked-out bar would doubtlessly be slightly lower than the strains in adjacent bars at the locations of a crack running through the blockout. These latter strains should be the representative strains used in moment computations. The possibility of such a phenomenon having any significant effect on results was, for all practical purposes, eliminated by conducting tests on one girder stem with a special type of gage. These tests clearly demonstrated that the measured strains in the lower bars corresponded accurately with the vertical strain distribution observed in the stem.

A fourth possibility may be considered in that the strain distribution assumed between stems and midbays may not represent the true distribution. The differences exhibited between stem and midbay strains were much larger than theoretical considera-

tions would indicate. The strain distribution in the intervening bars would have to be radically different from the parabolic distribution assumed, however, to produce any significant increase in computed resisting moments.

Much of the evidence observed in the box girder project favors an explanation of the discrepancy between computed total resisting moments and known external moments on the basis of results of some research work on flat slabs completed in recent years at the University of Illinois. In the course of this work it was observed that a reinforced concrete beam loaded into the cracking range and subsequently unloaded, would, on reloading, behave like an uncracked section, its stress-strain curve approximately paralleling the curve obtained before first cracking. It is hypothesized that, when the cracked structure is unloaded, cracks in the concrete do not close completely, leaving residual stresses in the tensile reinforcement which produce compressive stresses against whatever material is preventing closing of the cracks. Steel strains measured in the reinforcement during subsequent reloading of the beam, lacking consideration of these residual stresses, would be lower than strains commensurate with the moments applied to the beam.

Evidence favoring this explanation is furnished by the fact that, as will be noted below, when the steel stresses are eliminated from consideration in moment calculations by computing the moments of the compressive total stresses about the computed location of the tensile total stress resultants, the summation of computed resisting moments in the five girders is very nearly equal to the known acting moment. The fact that the computed total compressive stress across the transverse box girder section greatly exceeds the total tensile stress also favors the hypothesis that unmeasured residual stresses exist in the reinforcing steel. Lastly, the configuration of the oscillographic traces of strain in the lower slab reinforcing steel favors this hypothesis. If the phenomenon which keeps the cracks in the concrete from closing also permits the existence of temporary compressive stresses in the cracked area, the residual stresses in the tensile reinforcing steel would, in effect, cause the beam to behave like a partially prestressed beam, increasing the moment of inertia with respect to that of the fully cracked beam and lowering the neutral axis. As the beam is reloaded and the residual stresses are overcome, the cracks will re-open until the load reaches its former maximum value, when the beam again acts as a fully cracked section. This behavior would be manifested by a rising neutral axis, a decreasing moment of inertia, and an increasing "fiber distance" for the reinforcement. Under such circumstances, a linear change in bending moment would be accompanied by a curvilinear increase in reinforcement bending strains.

The influence line for bending moment or strain in a simple beam traversed by the two-axle test vehicle would normally be expected to be a broken line comprising the graphical summation of two dissimilar triangles whose vertices are displaced horizontally from one another by the wheelbase of the vehicle. The oscillographic traces in rare instances did assume such a configuration; however, in the general case, these traces exhibited a series of curvilinear traces with upward concavity, such as would be expected if the aforementioned phenomenon existed.

Unfortunately, at the time the oscillographic data were reduced, the possibility of such a phenomenon was not anticipated and the actual trace displacements were assumed to represent the strain patterns. In retrospect, it appears that the lower layer steel strains for each beam might more logically have been obtained by constructing an idealized influence line, based on the measured axle reactions, wheelbase, and bridge dimensions, on each oscillographic trace for which strains in a given gage reached the maximum strain in the course of the test. The ratios of influence line ordinates to trace displacements for various moments could then be used to correct the traces for any vehicle traverse. For one oscillographic trace treated in this manner, it was found that the strain at the $^{5}/_{12}$ths point, with the rear axle of the test vehicle at midspan, was increased by 30 percent.

It might reasonably be expected that, if this phenomenon did exist, the residual stresses after first loading would be readily observable on plots of dead load strain as functions of time and that overcoming these residual stresses would result in a delay in the appearance of strains on the oscillographic trace. Neither of these phenomena was

explicitly observable; however, it should be noted that these residual strains would be most pronounced at a crack but would be averaged out over a considerable length where the gages were blocked out or extensively waterproofed. Moreover, the aforementioned curvilinear configuration of the oscillographic traces does, in effect, constitute a delayed appearance of strain, though lacking the more abrupt nature which might be expected if the strain were measured at a crack.

Any of the five effects mentioned constitutes a possible contributing factor to the discrepancy between external and internal moment. Little evidence exists among the prototype strains for the existence of some of them; insufficient instrumentation precludes the elimination of others from consideration. The best evidence points to the fifth reason given, and the excellent agreement noted between total external moment and total resisting moment based on compressive total stresses only, favors this argument. To avoid any loopholes, however, four sets of girder resisting moments were calculated, using various assumptions, to cover the various possibilities.

The first set of values was established from the raw test data with little modification. Mean strains in the tensile reinforcing bars, assuming parabolic distribution, and measured strains in compressive reinforcement were used in conjunction with laboratory calibrations to establish total steel stresses. Mean strains in the concrete slab were multiplied by elastic moduli determined from tests on unreinforced control beam specimens poured simultaneously with the slab and subjected to a similar environment. Resulting values of resisting moments are given in Table 9 and shown in Figure 25 for test vehicles in hypothetical positions 4.10 and 11.43, with the rear axle at midspan. In all cases, such curves were drawn for the aforementioned critical locations and for the rear axle at the quarterspan and at midspan. Only typical curves will be included herein.

The discrepancy between computed total resisting moment and known acting moment is roughly 25 percent for this case. Total computed compressive stresses are significantly larger than computed total tensile stresses across the transverse sections

TABLE 9

COMPUTED LIVE LOAD RESISTING MOMENTS AT $^5/_{12}$ POINT OF SPAN[a]

Phase	Position Comb.	Resisting Moment (kip-ft)						E_c ($\times 10^3$ ksf)
		A	B	C	D	E	Total	
II	4.10	204	293	308	308	219	1,332	439.2
	+							
III	12.30	222	311	313	320	231	1,397	469.4
V	-	162	257	261	265	169	1,114	522.7
II	4.10	206	297	311	305	215	1,334	439.2
	+							
III	11.93	224	314	314	318	228	1,398	469.4
V	-	164	260	261	264	167	1,116	522.7
II	4.10	208	299	313	304	212	1,336	439.2
	+							
III	11.43	226	316	315	315	225	1,397	469.4
V	-	165	262	261	261	164	1,113	522.7

[a]Based on unmodified strain data and control beam moduli, rear wheels at midspan.

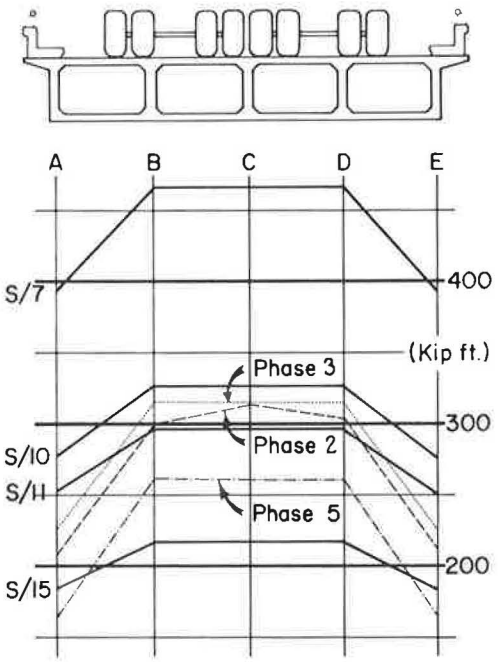

Figure 25. Computed live load resisting moments for two test vehicles in hypothetical transverse positions 4.10 and 11.43 (critical for center girder), with rear axle at midspan, taken about experimental neutral axis and based on control beam moduli.

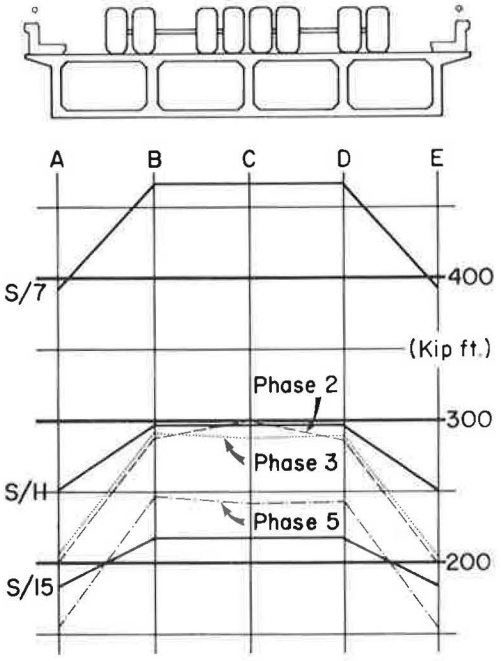

Figure 26. Computed live load resisting moments for two test vehicles in hypothetical transverse positions 4.10 and 11.43 (critical for center girder), with rear axle at midspan, taken about experimental neutral axis, with concrete moduli reduced to effect static balance between total tensile and compressive stresses.

studied. Two possible alternatives exist to effect static balance of the total stresses across the transverse section: (a) by decreasing the total computed compressive stress; or (b) by increasing the total computed tensile stress.

For the second set of resisting moments, the concrete modulus was assumed at a lower value than that measured for the control beams to effect static balance of total stresses by decreasing the total compressive stress. The control beams were, of necessity, tested in a much lower stress range than that to which the deck slab was subjected, possibly producing a higher figure for effective modulus. In addition, if it were possible for transverse deck cracks to exist in the high compressive stress field due to differential shrinkage of the deck slab against the restraint of the stems, the necessity for closing these cracks under live loading would reduce the effective modulus from that measured for the control beams. Resisting moments computed for the lower modulus are given in Table 10 and shown in Figure 26. Although static balance is established for total stresses by this method of computation, the discrepancy between external and internal moments is increased to 30 percent.

In the third calculation, resisting moments were computed explicitly in terms of concrete stresses using the control beam moduli in conjunction with measured strain patterns in the concrete and computing moments about the lower slab reinforcement. This method of calculation eliminates consideration of the tensile reinforcement stresses, assuming that these measured stresses are unrepresentative for reasons discussed previously. Results are given in Table 11 and shown in Figure 27. The discrepancy between internal and external moments is decreased to 8 percent for Phase II and 2 percent for Phase III.

TABLE 10

COMPUTED LIVE LOAD RESISTING MOMENTS AT $^5/_{12}$ POINT OF SPAN[a]

Phase	Position Comb.	Resisting Moment (kip-ft)						E_c ($\times 10^3$ ksf)
		A	B	C	D	E	Total	
II	4.10	195	281	295	294	207	1,272	351.8
	+							
III	12.30	200	286	286	293	208	1,273	353.9
V	-	150	240	241	247	156	1,034	353.9
II	4.10	197	284	297	291	204	1,273	351.8
	+							
III	11.93	202	288	287	291	205	1,273	353.9
V	-	151	239	237	246	155	1,028	353.9
II	4.10	201	289	299	287	199	1,275	351.8
	+							
III	11.43	204	290	288	289	202	1,273	353.9
V	-	153	245	241	243	152	1,034	353.9

[a]With concrete moduli reduced to produce static balance of total stresses, rear wheels at midspan.

TABLE 11

COMPUTED LIVE LOAD RESISTING MOMENTS AT $^5/_{12}$ POINT OF SPAN[a]

Phase	Position Comb.	Resisting Moment (kip-ft)						E_c ($\times 10^3$ ksf)
		A	B	C	D	E	Total	
II	4.10	282	342	370	357	301	1,652	439.2
	+							
III	12.30	313	364	376	378	328	1,759	469.4
II	4.10	286	346	375	354	297	1,658	439.2
	+							
III	11.93	317	366	377	375	325	1,760	469.4
II	4.10	291	350	380	351	291	1,663	439.2
	+							
III	11.43	320	370	379	370	320	1,759	469.4

[a]Based on control beam moduli and taken about resultant of total tensile stress.

In the fourth set of calculations, the resisting moments for individual stringers in each of the previously mentioned calculations were arbitrarily increased by the ratio of the known external moment to the summation of individual stringer moments. Envelopes of resulting maximum moments for each stringer are shown in Figures 28a and 29a for the rear axle at midspan and quarterspan, respectively. The latter calculation was not extended to Phase V because of the indeterminate nature of the contribution of the barrier curbs and railings to the individual stringers.

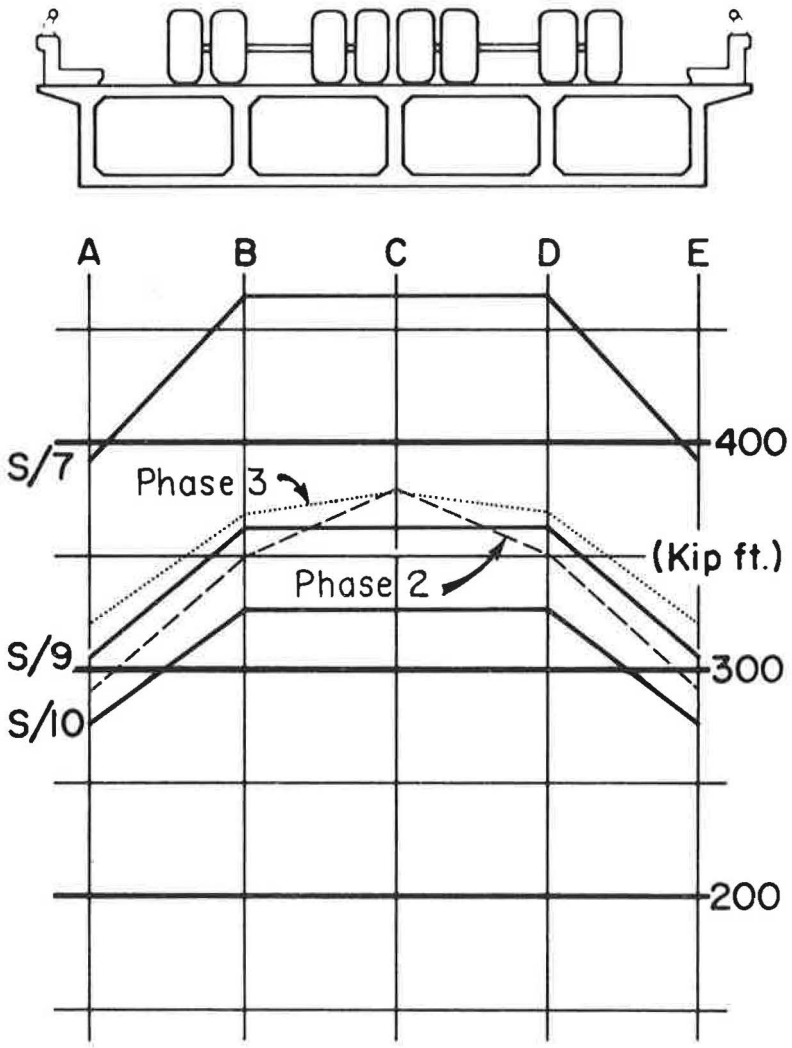

Figure 27. Computed live load resisting moments for two test vehicles in hypothetical transverse positions 4.10 and 11.43 (critical for center girder), with rear axle at mid-span, taken about resultant of total tensile stresses and using control beam moduli.

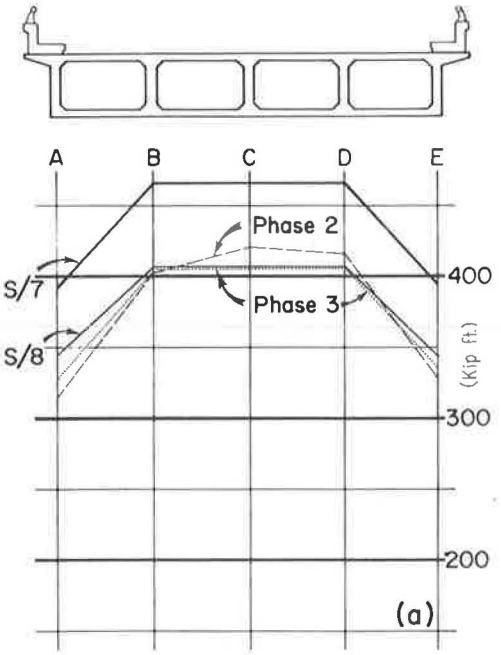

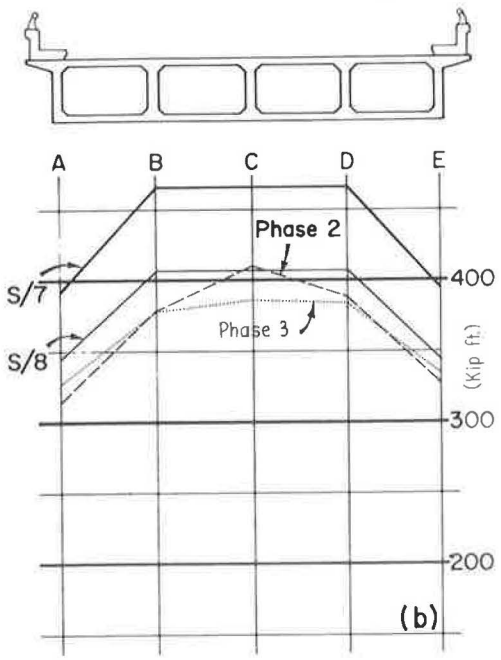

Figure 28(a). Envelopes of maximum augmented live load resisting moments for two test vehicles in hypothetical transverse positions critical for various girders, and with rear axle at midspan; and (b) using only moment of total compressive stresses about tensile resultant location.

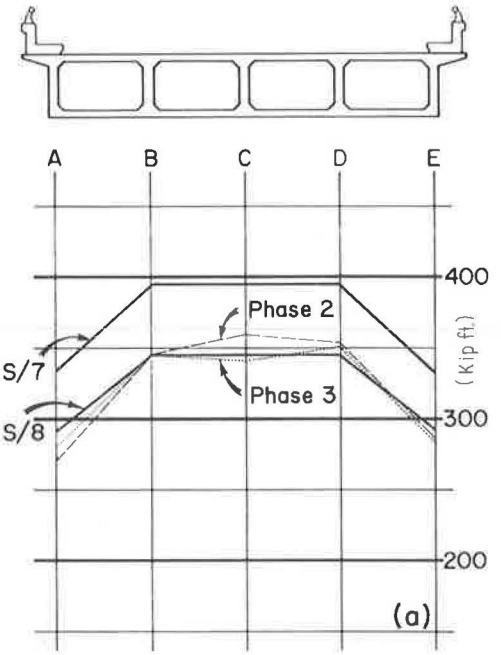

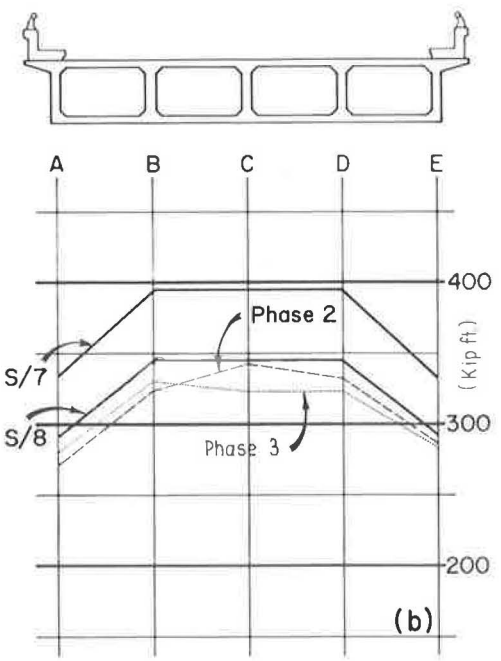

Figure 29(a). Envelopes of maximum augmented live load resisting moments for two test vehicles in hypothetical transverse positions critical for various girders, and with rear axle at quarterspan; and (b) using only moment of total compressive stresses about tensile resultant location.

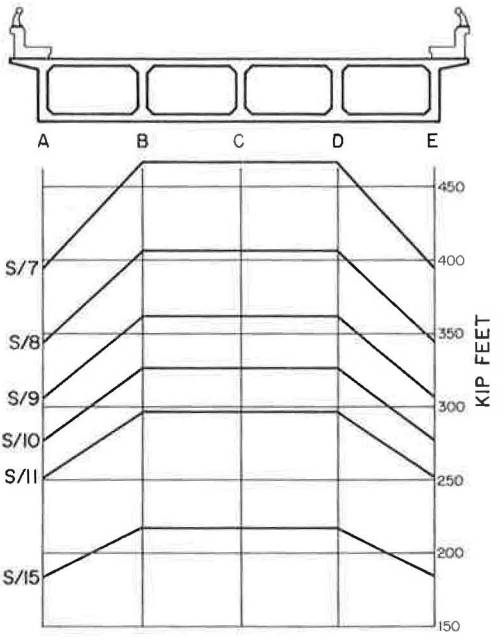

Figure 30. Live load resisting moments for various distribution factors, rear axle at midspan.

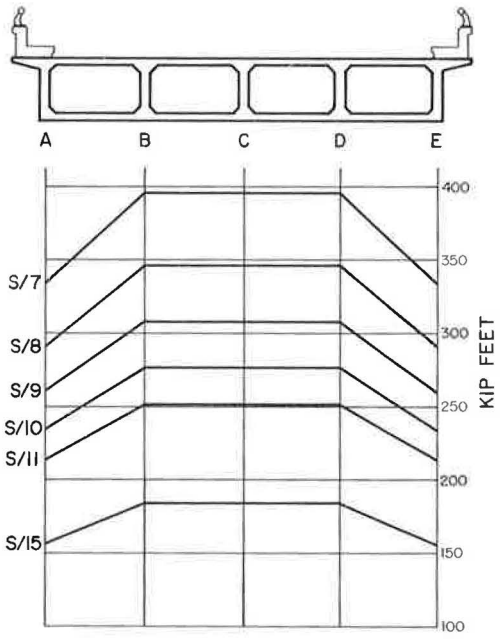

Figure 31. Live load resisting moments for various distribution factors, rear axle at quarterspan.

TABLE 12

EMPIRICAL VALUES OF DISTRIBUTION FACTOR, K

Stringer	No. of Wheel Lines, WL	WL/S	$\frac{WL/S}{W_e/S}$	K
	(a) Phase II[a]			
A	$\frac{314}{449} = 0.699$	0.096	0.114	8.77
B	$\frac{407}{449} = 0.906$	0.125	-	8.00
C	$\frac{421}{449} = 0.938$	0.129	-	7.75
D	$\frac{416}{449} = 0.927$	0.128	-	7.82
E	$\frac{327}{449} = 0.728$	0.100	0.118	8.48
	(b) Phase III[a]			
A	$\frac{327}{449} = 0.728$	0.100	0.118	8.48
B	$\frac{409}{449} = 0.911$	0.126	-	7.94
C	$\frac{406}{449} = 0.904$	0.125	-	8.00
D	$\frac{413}{449} = 0.920$	0.127	-	7.88
E	$\frac{335}{449} = 0.746$	0.103	0.122	8.20
	(c) Phase II[b]			
A	$\frac{314}{449} = 0.699$	0.096	0.114	8.78
B	$\frac{378}{449} = 0.842$	0.116	-	8.62
C	$\frac{411}{449} = 0.915$	0.126	-	7.94
D	$\frac{388}{449} = 0.864$	0.119	-	8.40
E	$\frac{327}{449} = 0.728$	0.100	0.118	8.48
	(d) Phase III[b]			
A	$\frac{327}{449} = 0.728$	0.100	0.118	8.48
B	$\frac{378}{449} = 0.842$	0.116	-	8.62
C	$\frac{387}{449} = 0.862$	0.119	-	8.40
D	$\frac{386}{449} = 0.860$	0.119	-	8.40
E	$\frac{335}{449} = 0.746$	0.103	0.122	8.19

[a]Based on envelopes of maximum augmented values of resisting moments computed by four methods.

[b]Based on maximum augmented values of resisting moments of total concrete stresses about location of tensile resultant.

TABLE 13

EXPERIMENTAL LIVE LOAD MOMENTS[a]

Girder	Resisting Moment (kip-ft)	Proportion of Total
A	208	0.156
B	299	0.224
C	313	0.234
D	304	0.228
E	212	0.159
Total	1,336	-

[a]From Table 9, Phase II; Position 4.10 + 11.43, rear axle at midspan, (calculated from control beams for Phase II).

TABLE 14

EXPERIMENTAL LIVE LOAD MOMENTS[a]

Girder	Resisting Moment (kip-ft)	Proportion of Total
A	291	0.175
B	350	0.210
C	380	0.228
D	351	0.211
E	291	0.175
Total	1,663	-

[a]Moments of compressive resultants about tensile resultant, Phase II, from Table 11, Phase II; Position 4.10 + 11.43, rear axle at midspan, E_c = 439,200 ksf (calculated from control beams for Phase II).

TABLE 15

EXPERIMENTAL LIVE LOAD MOMENTS[a]

Girder	Resisting Moment (kip-ft)	Proportion of Total
A	320	0.182
B	370	0.210
C	379	0.215
D	370	0.210
E	320	0.182
Total	1,759	-

[a]Moments of compressive resultants about tensile resultant, Phase III, from Table 11, Phase III; Position 4.10 + 11.43, rear axle at midspan, E_c = 439,200 ksf (calculated from control beams for Phase III).

TABLE 16

EXPERIMENTAL LIVE LOAD MOMENTS[a]

Girder	Resisting Moment (kip-ft)	Proportion of Total
A	201	0.157
B	289	0.227
C	299	0.235
D	287	0.225
E	199	0.156
Total	1,275	-

[a]Position 4.10 + 11.43; rear axle at midspan; E_c = 351,800 ksf (value required to satisfy statics for total longitudinal stresses).

A similar augmentation was performed using only the moment of the total compressive stresses about the tensile resultant location. Envelopes are plotted in Figures 28b and 29b for the rear axle at midspan and quarterspan, respectively.

For comparison purposes, each of the previous graphs depicts the resisting moment in each girder as it would be computed for a fractional distribution of S/7. In addition, Figures 30 and 31 depict computed moments for several other fractional distributions up to S/15.

The aforementioned maximum bending moments in the stringers may be translated into more familiar design terms. If S/K is the number of wheel lines distributed to each interior stringer for an average stringer spacing, S, and $(W_e/S)(S/K)$ is the corresponding factor for the exterior stringer, where W_e is one-half the panel width plus the width of slab overhang; the factor, K, may be computed as shown in Table 12. The moment per wheel line, with rear axle at midspan = 449 ft-kips. A similar calculation

TABLE 17

THEORETICAL LIVE LOAD MOMENTS[a] (First Method)

Girder	Resisting Moment (kip-ft)	Proportion of Total
A	261	0.144
B	430	0.237
C	444	0.244
D	423	0.233
E	258	0.142
Total	1,816	-

[a]Position 4.10 + 11.43; rear axle at midspan; E_c = 432,000 ksf.

TABLE 18

THEORETICAL LIVE LOAD MOMENTS[a] (Second and Third Methods)

Girder	Resisting Moment (kip-ft)	Proportion of Total
A	280	0.153
B	420	0.229
C	430	0.235
D	420	0.229
E	280	0.153
Total	1,830	-

[a]Position 4.10 + 11.43; rear axle at midspan; E_c = 432,000 ksf.

TABLE 19

EXPERIMENTAL LIVE LOAD MOMENTS[a]

Girder	Resisting Moment (kip-ft)	Proportion of Total
A	204	0.153
B	293	0.220
C	308	0.231
D	308	0.231
E	219	0.164
Total	1,332	-

[a]From Table 9, Phase II; Position 4.10 + 12.30; rear axle at midspan; E_c = 439,200 ksf (calculated from control beams for Phase II).

TABLE 20

EXPERIMENTAL LIVE LOAD MOMENTS[a]

Girder	Resisting Moment (kip-ft)	Proportion of Total
A	282	0.171
B	342	0.207
C	370	0.224
D	357	0.216
E	301	0.182
Total	1,652	-

[a]Moments of compressive resultants about tensile resultants, Phase II, from Table 11, Phase II; Position 4.10 + 12.30, rear axle at midspan, E_c = 439,200 ksi (calculated from control beams for Phase II).

was made using only augmented moments of total compressive stresses about the location of the tensile resultant. Values of K for this calculation are also listed in Table 12.

Selected results of calculations of experimental live load moments are listed in Tables 13 through 18. Table 13 lists the ratios of individual stringer to total moments computed by the aforementioned first method and listed in Table 9. Similar ratios for moments of total compressive stresses about tensile resultant locations are listed in Tables 14 and 15 for Phases II and III, respectively—the moments in the latter two tables were taken from Table 11. Table 16 lists these ratios for moments computed by the second method, wherein all moments are increased by the ratio of known external moment to computed internal moment. Tables 19 through 22 list similar ratios for a different critical position of the test vehicles.

It should be emphasized that the results shown are for a structure with the particular configuration of the test structure, and that these results may require modification for structures with other configurations if theoretical considerations so indicate.

TABLE 21

EXPERIMENTAL LIVE LOAD MOMENTS[a]

Girder	Resisting Moment (kip-ft)	Proportion of Total
A	313	0.178
B	364	0.207
C	376	0.214
D	378	0.215
E	328	0.186
Total	1,759	-

[a]Moments of compressive resultants about tensile resultants, Phase III, from Table 11, Phase III; Position 4.10 + 12.30, rear axle at midspan, E_c + 439,200 ksf (calculated from control beams for Phase III).

TABLE 22

EXPERIMENTAL LIVE LOAD MOMENTS[a]

Girder	Resisting Moment (kip-ft)	Proportion of Total
A	195	0.154
B	281	0.221
C	295	0.232
D	294	0.231
E	207	0.163
Total	1,272	-

[a]Position 4.10 + 12.30; rear axle at midspan; E_c = 351,800 ksf (value required to satisfy statics for total longitudinal stresses).

THEORETICAL ANALYSIS

In order that the results of field and model studies might be extended to permit application of these results to structures varying in configuration from the field prototype, certain analytical procedures were investigated. The first method comprises an attempt to apply a distribution procedure developed by Newmark (3). Because some of the assumptions used in Newmark's development do not hold true in the case of the box girder, some modifications of the method have been required. The third method entails an application to the box girder of folded plate equations developed by Goldberg and Leve (4), using matrix algebra. The second method combines portions of the first and third methods, treating the transverse rigidity phase by Newmark's method, and the longitudinal rigidity phase by folded plate equations. Whereas the mathematical approach used in the second method differs considerably from that used in the third, the results of these two solutions are the same.

Because all three procedures involve much tedious arithmetic, the use of an electronic computer is essential. The computational burden connected with the work described herein was, in large measure, carried out by programming in FORTRAN language for an IBM 704 owned by the Division of Highways.

Description of Analytical Procedures

The distribution procedure developed by Newmark was designed for application to slabs on steel I-beams, wherein the assumption can be made that there exists negligible transfer of longitudinal shear at the beam-slab interface. Transverse slab moments and shears are distributed by the moment distribution method, modified for application to the slab elements. Effects of the torsional rigidities of the supporting beams may be included. The analysis may, in effect, be separated into two phases, in which the effects of transverse slab rigidity and of longitudinal girder rigidities are evaluated separately.

This brief description evidences some of the shortcomings of the method in its application to the box girder. For one thing, the torsional rigidity of the supporting beams becomes indeterminate in the box girder section due to the restraint at the bottom of the web resulting from the presence of the lower slab. An attempt has been made to surmount this difficulty by treating the webs and lower slab in a manner comparable to that used by Newmark for the top slab. The transverse section thus becomes analogous

to a Vierendeel truss with rigid joints, with the slabs and webs comprising the truss members.

A second difficulty arises from the fact that the webs are integral with the upper and lower slabs, and longitudinal shear is inevitable at the joints. Although the assumption of no longitudinal shear transfer is basic in Newmark's method, he suggests as an approximation, where "T-beam" action is present, the use of a modified moment of inertia in the calculation of the longitudinal girder stiffness. In the first method, the moment of inertia of the entire I-section between vertical planes at the midbays has been used in the computation of the longitudinal stiffness. This expedient, however, does not adequately take into account the longitudinal rigidity of the closed box section; this is believed to be the reason for the poor results from the use of this method. In the second method, the longitudinal stiffness is treated by use of those folded plate equations treating the membrane stresses, with considerably improved results.

The third method does not deal with transverse and longitudinal rigidities in separate steps but employs all of the folded plate equations to permit evaluation of a stiffness matrix for the section. This procedure provides a convenient method for evaluation of girder deflections and internal stresses for various applied loads.

An ordered description of steps involved in the three procedures follows. Outlines of the first and second methods are combined because the first phase of each method, considering only the effects of transverse rigidity, is the same.

Analytical Procedures—First and Second Methods

1. Resolve the external loading forces into component terms of a Fourier series. Use equations furnished by Newmark (3) where applicable. (It is convenient to defer inclusion of the sine terms in the series expansions and to deal only with amplitudes of the forces until the final stages of the analysis.)
2. Replace the transverse box girder section with an "analogous Vierendeel truss" with vertical sections of the slabs and webs replaced by the truss members. It is assumed that the slabs are framed into diaphragms at the bearings only and that these end diaphragms provide only simple support without moment restraint in a longitudinal direction.
3. Compute stiffness and carry-over characteristics for each member of the analogous truss for determination of fixed end moments and reactions. Because these factors apply to truss members which are, in reality, sections of slabs, they will differ numerically from similar factors for beams. Values may be found by interpolation from tables provided by Newmark (3), or they may be computed from equations furnished for the purpose. Although these coefficients include hyperbolic functions for which accurate tables are not always available, computation by electronic computer makes the use of the equations more convenient than use of Newmark's tables.
4. Using the coefficients from Step 3 and the loading components from Step 1 for known values of the loading, fixed edge moments and reactions may be computed for each value of the Fourier module.
5. Assume that the slabs are inextensible between joints. At the bottom of each web and at one end of each slab, introduce constraints which permit longitudinal movements and joint rotations but prevent transverse or vertical translations.
6. Compute unbalanced moments at each joint and, by successive relaxations, distribute moments around the analogous truss using the carry-over factors from Step 3.
7. Calculate modifications of the fixed end reactions resulting from the relaxation of the joints in the course of distributing moments. The analogy with the Vierendeel truss breaks down here because the reaction changes cannot be computed by statics. A description of the applicable procedure is given by Newmark (3).
8. Summation of the modified fixed end reactions along horizontal or vertical planes will produce a total of seven external reactions at the points of constraint. The loading producing these reactions may be replaced by a set of seven hypothetical external loads (R_{10}, R_{20}, . . . , R_{70}) acting at the panel points. These loads are equal and opposite to the external reactions (Fig. 32).

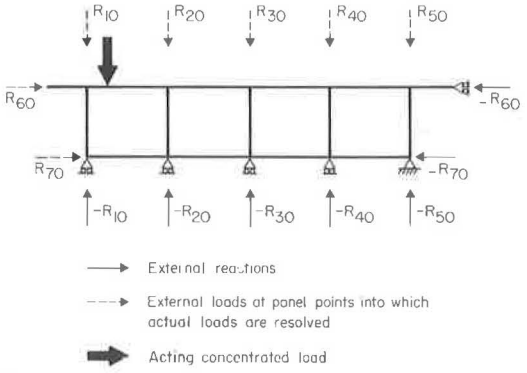

Figure 32. Resolution of external actions with joints restrained.

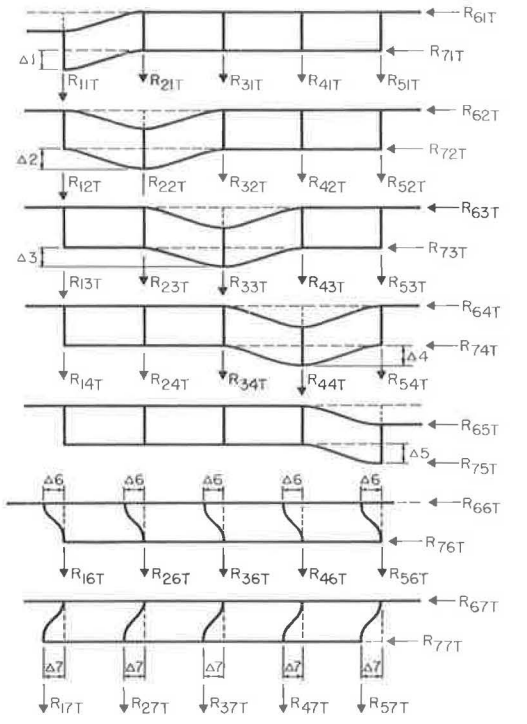

Figure 33. Hypothetical displacement patterns assumed in analysis: transverse rigidity phase.

9. Assume a set of seven independent patterns of deflection, in which each girder stem (two joints) and each slab (five joints each) are deflected through known distances.

10. Compute a new set of fixed end moments and reactions commensurate with each deflection pattern. This calculation will require coefficients applicable to slab deflections computed from Step 3.

11. Distribute unbalanced moments as before and compute the changes in the new fixed end reactions due to joint relaxations.

12. Compute a second set of reactions (R_{11T}, R_{21T}, ..., R_{71T}; R_{12T}, R_{22T}, ..., R_{72T}; etc.) required to hold the analogous truss in equilibrium in each distorted configuration (Fig. 33). (R_{ij} is the reaction at panel point i due to a deflection at panel point j.)

13. The reactions determined in Step 12 are based on the assumption that the structure has large transverse rigidity compared to its longitudinal rigidity; the first and second methods are identical to this point.) A second component of reaction must be calculated at each panel point assuming that the structure has large longitudinal rigidity compared to its transverse rigidity. Superposition of the two reaction components will result in reactions required to produce the deflected configurations for a structure with rigidity in both directions.

14. The method used to compute the reaction components for the structure with large longitudinal rigidity constitutes the basic difference between the first and second methods.

a. First Method.—The individual girders are assumed to be cut at the midpoints of the bays by vertical planes or at the mid-depths of the stems by horizontal planes (Fig. 34). Girder stiffnesses are computed and multiplied by the same deflections used in Step 9. Because this girder stiffness is a function of the girder moment of inertia, this method permits the use of any desired section, be it cracked or uncracked. The procedure possesses the disadvantage that it neglects the longitudinal rigidity of the closed box section, which may be appreciable.

b. Second Method.—The webs and slabs are assumed to be membranes which can sustain longitudinal shears and normal stresses but no transverse moments or shears; the latter two components are covered in the first step for both methods. Values of S, the longitudinal shears, and of N, the normal stresses, will depend on the longitudinal displacements of the joints, u, and transverse displacements, v. Goldberg and Leve (4) have developed equations for N and S in terms of u and v. With values of v established for the seven aforementioned displacement patterns, it is possible, through use of these equations, to compute corresponding values of u by formulating equilibrium

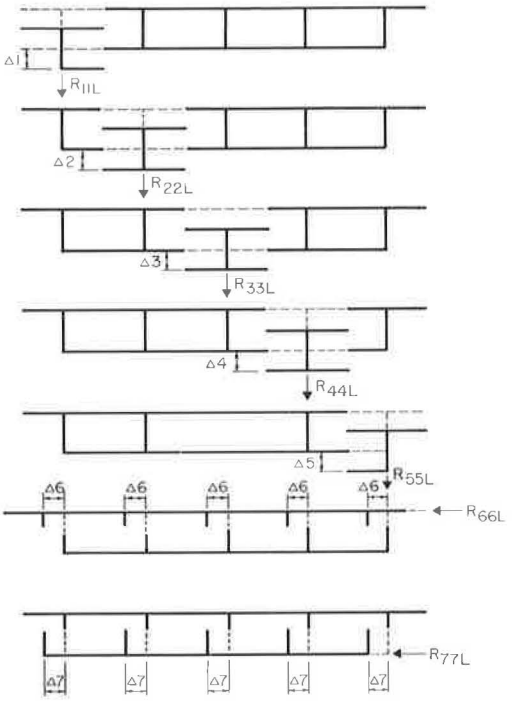

Figure 34. Hypothetical displacement patterns assumed in analysis: longitudinal rigidity phase.

equations for the longitudinal shears at each joint. The resulting values of u, together with the corresponding assumed values of v, may be employed to determine the N forces for each member at the joints. The N forces may be summed along vertical and horizontal lines to produce the second components of reactions, R_{11L}, R_{21L}, ..., R_{71L}; R_{12L}, R_{22L}, ..., R_{72L}; etc. This method permits an evaluation of the longitudinal shears at the joints but possesses the disadvantage that it deals purely in terms of the gross concrete section.

15. Values of R_{ijT} established from Step 12 for the structure with assumed negligible longitudinal rigidity and values of R_{ijL} established by one of the two methods in Step 14 for a structure with assumed negligible transverse rigidity may be summed to produce the external actions required to hold a structure with rigidity in both directions in the assumed deflected configurations. The internal actions resisting these displacements will be equal and opposite to the external actions:

$$R_{11} = -\left(R_{11L} + R_{11T}\right)$$

$$R_{21} = -\left(R_{21L} + R_{21T}\right), \text{ etc.} \quad (3)$$

16. If, under a given loading condition, k, the deflections of the girders and slabs are Δ_{1k}, Δ_{2k}, ..., Δ_{ik}, ... Δ_{7k}, the total internal action at Joint i is the summation of the component internal actions at Joint i due to deflections at the other joints. Expressed as an equation, the total internal resisting force at Joint i is:

$$R_{i1}\,\Delta_{1k} + R_{i2}\,\Delta_{2k} + \ldots + R_{i7}\,\Delta_{7k} \quad (4)$$

For equilibrium to exist, the internal action at each panel point must be equal and opposite to the external load at the same panel point, the latter having been computed in Step 8. Thus,

$$-R_{10} = R_{11}\,\Delta_{1k} + R_{12}\,\Delta_{2k} + \ldots + R_{17}\,\Delta_{7k}, \text{ etc.}, \quad (5)$$

or

$$R_{10} = \left(R_{11L} + R_{11T}\right)\Delta_{1k} + \left(R_{12L} + R_{12T}\right)\Delta_{2k} + \ldots + \left(R_{17L} + R_{17T}\right)\Delta_{7k} \quad (6)$$

Similar equations may be written for each of the seven girders (slabs), producing seven equations in seven unknown deflections for each loading condition.

17. The seven equations are solved for the seven unknown deflections of the girders and slabs for each condition of loading. The procedure must be repeated for a sufficient number of values of the Fourier module to result in convergence.

18. At this point the proper sine functions are applied as factors to component terms of the Fourier series and summations are calculated to produce the total theoretical deflections at each panel point. These deflections may then be employed to compute the girder resisting moments or the desired slab stresses (depending on the method used) for comparison with empirically determined values. Results of the first method are in terms of individual girder resisting moments, whereas the second and third methods result in longitudinal slab stresses, there being no way to evaluate resisting moments directly by these two methods. Combined effects of the separate wheel loadings may be most conveniently evaluated by making the calculations for a single concentrated load in a large number of positions and then evaluating the effects of the measured wheel reactions through the use of influence lines and surfaces.

Solution by Matrix Formulation of Folded Plate Equations—Third Method

1. The folded plate equations published by Goldberg and Leve (4) are in the general form:

$$P_{ijm} = F_{Fijm} + Q(=\Sigma C\delta) \tag{7}$$

where P_{ijm} is a final edge force, F_{Fijm} is a fixed edge force, and Q represents the internal edge force due to edge displacements. For equilibrium to exist at a joint, the final edge forces and moments produced by all members framing into the joint must sum to zero. Therefore, a relationship may be established between the fixed edge forces produced by external forces acting on the plates and the forces resulting from edge displacements. It is also possible to establish a relationship between the external joint displacements and the internal edge displacements. The external system having forces and displacements are conveniently related to a coordinate system having a constant orientation in space. The folded plate equations are related by Goldberg and Leve (4) to coordinate systems whose orientations vary with the orientations of the plates. The external forces and displacements are, in general, also designated in a different manner than are the internal forces and displacements. The fixed edge and external forces are related in the analysis through an equilibrium matrix:

$$\left[\Sigma F_{Fijm}\right] + [A][Q] = \left[\Sigma P_{ijm}\right] = 0 \tag{8}$$

The internal edge displacements, δ, are related to the joint displacements, Δ, by the geometry matrix:

$$[\delta] = [B][\Delta] \tag{9}$$

The [A] and [B] matrices are formulated so that one is the transpose of the other.

2. A stiffness matrix is formulated to relate the internal edge forces to the internal edge displacements:

$$[Q] = [S][\delta] = [S][B][\Delta] = [S][A]^T[\Delta] \tag{10}$$

and

$$[P] + [A][Q] = 0 \tag{11a}$$

$$[P] + [A][S][A]^T[\Delta] = 0 \tag{11b}$$

3. If the matrix product, $[A][S][A]^T$ is designated by the single matrix, [K],

$$[P] + [K][\Delta] = 0 \tag{12a}$$

and

$$[\Delta] = -[K]^{-1}[P] \tag{12b}$$

4. Substitution of Eq. 12b in Eq. 10 yields

$$[Q] = [S][A]^T\left(-[K]^{-1}[P]\right) \tag{13}$$

5. Final edge forces are represented by the summations of the fixed edge forces and the forces due to edge displacements.

6. Forces at any point within the plates may be evaluated through use of equations furnished by Goldberg and Leve (4).

7. To reduce the sizes of the matrices employed, symmetric and antisymmetric load systems are employed, the box section being split at the center web. A discussion of this treatment of loads is given by Newell (5). As applied to the box section, this treatment of loads has the following implications at Joints C and H, at the top and bottom of the center web:

a. Symmetric Case.—Displacements and rotations perpendicular to the plane of symmetry, and external forces producing shears parallel to the plane of symmetry are zero (Fig. 35). External moments and forces normal to the plane of symmetry, resulting from the hypothetical loads on the removed half of the structure, produce, in effect, built-in restraints which prevent the normal displacements and rotations. Because these external forces nullify similar but oppositely disposed forces in the half structure, these oppositely disposed forces need not appear in the F-matrix, nor do the zero displacements appear in the Δ-matrix. There are no bending moments or normal shears in the web, CH, but there may exist longitudinal shears and membrane stresses. Therefore, the stiffness factor used in computing S and N must be halved.

b. Antisymmetric Case.—Displacements parallel to the plane of antisymmetry, and forces and moments normal to the plane of symmetry are zero (Fig. 36). There exist vertical and longitudinal shears parallel to the plane of antisymmetry, resulting from the hypothetical antisymmetric loads, restraining the Joints C and H from movements parallel to the plane of antisymmetry. These external forces nullify similar but oppositely directed forces in the half structure, which need not be included in the F-matrix. Displacements parallel to the plane of antisymmetry are not included in the Δ-matrix. There exist no longitudinal shears or planar stresses in the center web, but there may exist transverse moments and shears. The transverse flexural stiffness used in computing M and V must be halved.

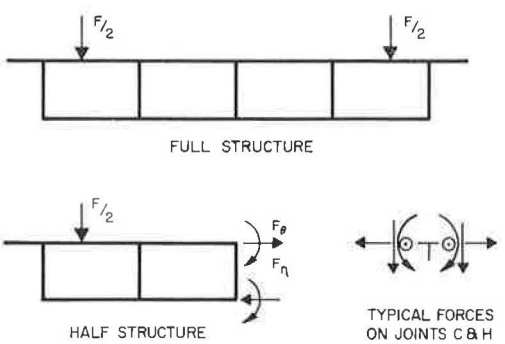

Figure 35. Force distribution for symmetric loading.

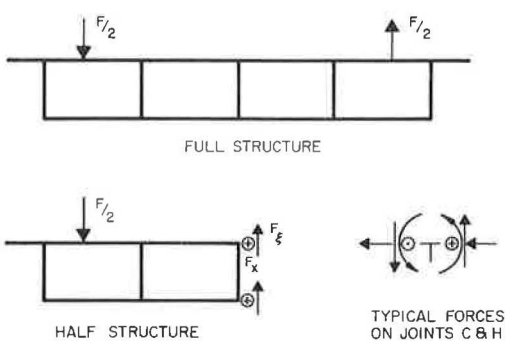

Figure 36. Force distribution for antisymmetric loading.

c. The displacements and internal forces may be found by superposing the results of the two cases.

As has been stated before, the mathematical work involved in the theoretical analysis was performed in large measure by an IBM 704 through the use of FORTRAN programs. The machine work entailed calculation of frame constants for slab components of the analogous Vierendeel truss, including distribution and carry-over factors for loads and displacements; calculation of coefficients for fixed edge moments and reactions; distribution of moments through the truss by the Bridge Department's Multi-story Frame Distribution Program; modification of fixed edge reactions due to joint relaxations during the distribution process; solution of simultaneous or matrix equations for panel point displacements; and calculation of resisting moments or longitudinal slab stresses. The actual mechanics of applying these methods are described only briefly herein. The theoretical methods will be discussed in more detail in a final project report.

For dead load, the calculations were made for the actual loads of the components of the structure (expressed, of course, in terms of their Fourier components). For live loads, calculations were first made for a 1,000-kip concentrated load placed on the upper slab at the fifth points of the bays. The results of these calculations were used to plot influence lines or surfaces of deflections, and resisting moments (first method) or longitudinal stresses (second and third methods). Transparent overlays depicting the test vehicle wheel locations in plan or section were used in conjunction with these charts to permit computation of deflections and resisting moments or stresses for the test vehicle in various transverse locations. In general, the calculations were made for two longitudinal locations of the vehicle, i.e., with the rear axle at the quarterspan and midspan, for comparison with the empirically determined values.

COMPARISON OF THEORETICAL AND EMPIRICAL RESULTS

To test the relative applicability of the three analytical methods employed, computed theoretical results were compared with values measured experimentally. Such comparisons may be made in several ways. Certain complications arise in establishing the comparisons.

Results of theoretical calculations are given in terms of resisting moments or longitudinal stresses, and deflections, whereas the experimental measurements comprised strains and deflections. Establishment of a comparison between any measurement and its theoretical counterpart requires knowledge of an effective modulus of elasticity for the concrete in the structure, which may be difficult to assess.

As noted earlier, measured strains and deflections do not accord fully with expectations based on idealized structural behavior. Dead load, total, tensile and compressive stresses, and external and internal moments may be made to satisfy static equilibrium principles simultaneously only by using a somewhat arbitrary system of longitudinal strain averaging and by assuming a relatively low value for effective concrete modulus. Live load, total, tensile and compressive stresses cannot be made to satisfy statics simultaneously, regardless of choice of concrete modulus. External and internal moments may be made nearly equal for experimental moduli if the moments of the total compressive stresses are computed about the locations of the total tensile stress resultant. The known external moments always exceed the summations of internal stringer resisting moments computed from strain patterns and measured concrete moduli or reinforcing steel calibration factors. By contrast, the various theoretical methods employed produce results complying with the principles of static equilibrium. Comparisons between actual, theoretical and measured strains and deflections will, therefore, be of less importance than comparisons of the relationships these individual values, translated into resisting moments, bear to their summations.

When comparisons are made between measured strains for the lower slab reinforcement and strains computed by the second and third analytical methods, consideration must be given to the fact that these methods deal with the gross concrete section. The problem has been treated herein by increasing the theoretical strains computed for the lower slab by the ratio of the gross area of the lower slab to the transformed area of the lower layer of reinforcing steel. This ratio is of smaller magnitude

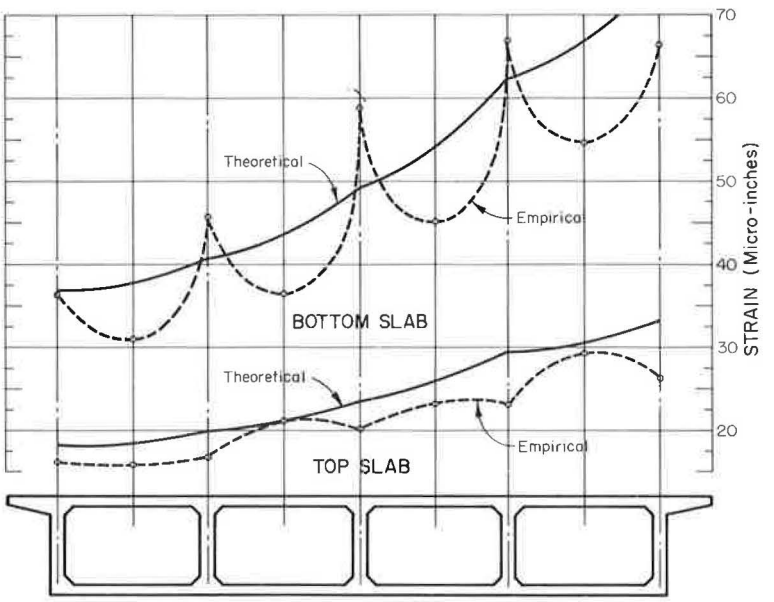

Figure 37. Comparison of theoretical and experimental live load strain distributions for test vehicle in transverse Position 13.

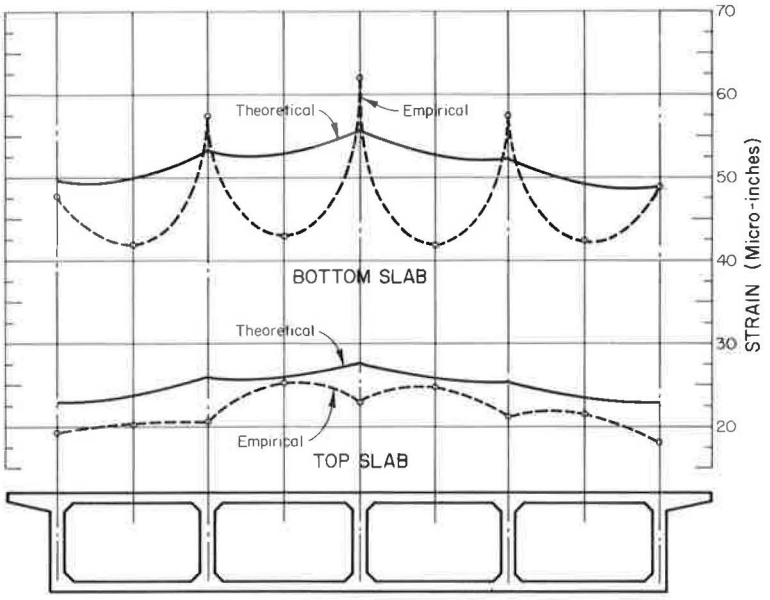

Figure 38. Comparison of theoretical and experimental live load strain distributions for test vehicle in transverse Position 7.

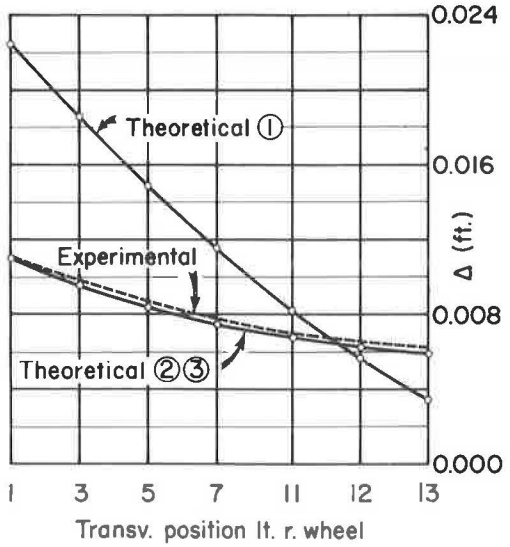

Figure 39. Comparisons of theoretical and experimental live load deflections as functions of transverse position of test vehicle; Girder A.

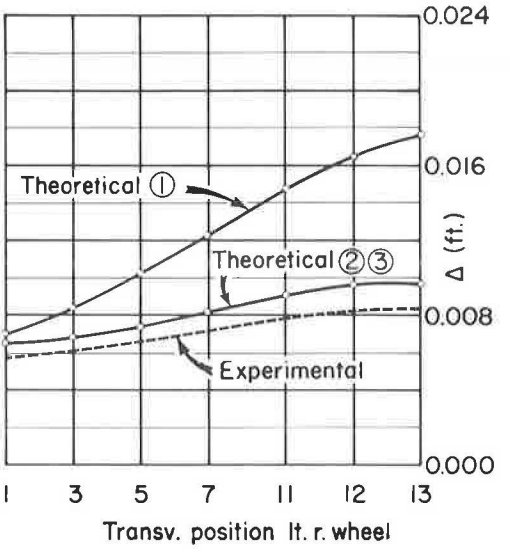

Figure 40. Comparisons of theoretical and experimental live load deflections as functions of transverse position of test vehicle; Girder D.

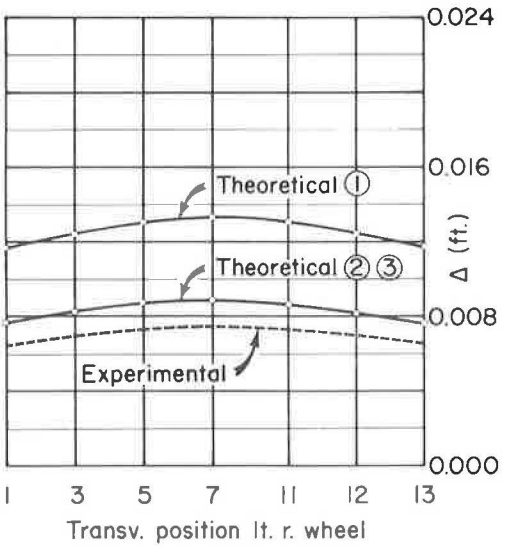

Figure 41. Comparisons of theoretical and experimental live load deflections as functions of transverse position of test vehicle; Girder C.

than it should be because a significant area of the concrete stems has been neglected. The discrepancies between theoretical and measured strains will, therefore, not appear commensurate with the discrepancies between measured and computed moments.

Because the folded plate equations do not take into consideration the orthotropy of the reinforced slab, this approximation is not rigorous. However, because the lower slab was cracked only transversely and the gross section is likely to be the applicable section for the other types of forces treated by the folded plate equations, the approximation, based on the assumption that all longitudinal stress computed for the lower slab is concentrated in the reinforcing steel, should closely predict the true strain pattern. In Figures 37 and 38, theoretical live load strains (the lower slab strains having been augmented as discussed previously) are compared with strains determined experimentally for the test vehicle in Positions 7 and 13.

Theoretical vs Empirical Live Load Deflections

Figures 39, 40 and 41 depict the comparisons between theoretical and measured deflections for the exterior, interior, and center girders. Deflections computed by the first method show very little agreement with the experimental values. Results of

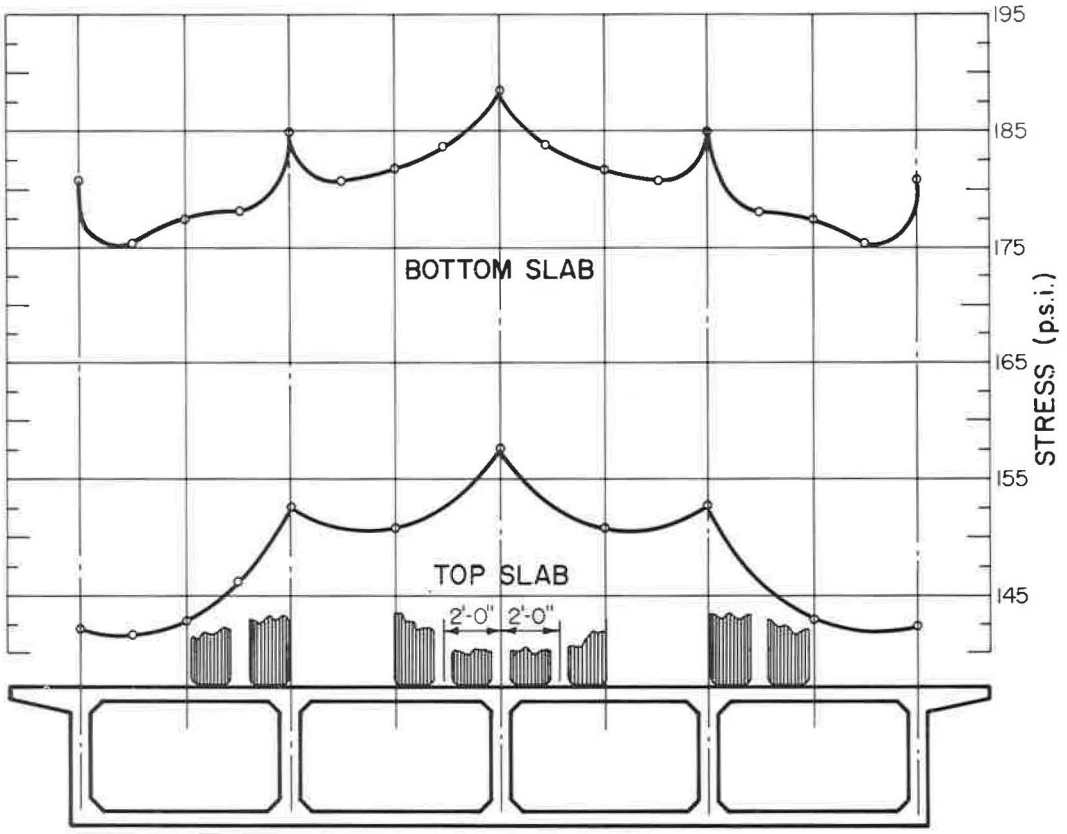

Figure 42. Theoretical live load stress distribution computed by third method for test vehicles in hypothetical positions 4.10 and 11.43 (critical for center girder), with rear axles at midspan.

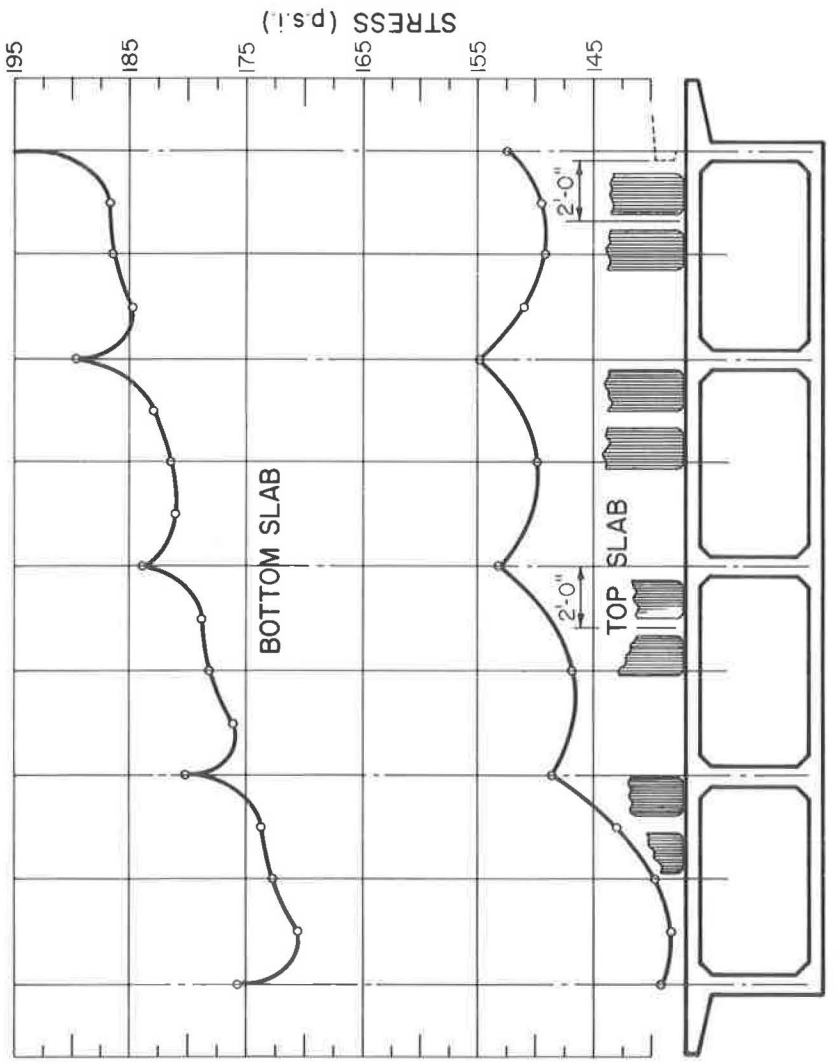

Figure 43. Theoretical live load stress distribution computed by third method for test vehicles in hypothetical positions 4.10 and 12.30 (critical for exterior girder), with rear axles at midspan.

TABLE 23

THEORETICAL LIVE LOAD MOMENTS[a] (First Method)

Girder	Resisting Moment (kip-ft)	Proportion of Total
A	238	0.131
B	403	0.222
C	423	0.233
D	448	0.247
E	301	0.166
Total	1,813	-

[a]Position 4.10 + 12.30; rear axle at mid-span; E_c = 432,000 ksf.

TABLE 24

THEORETICAL LIVE LOAD MOMENTS[a] (Second and Third Methods)

Girder	Resisting Moment (kip-ft)	Proportion of Total
A	273	0.150
B	408	0.223
C	420	0.230
D	427	0.234
E	298	0.163
Total	1,827	-

[a]Position 4.10 + 12.30; rear axle at mid-span; E_c = 432,000 ksf.

the second and third methods were plotted as one curve. Although trends of the latter and experimental curves show considerable parallelism, the magnitudes may differ by as much as 20 percent. Theoretical deflections were computed for an elastic modulus of concrete of 432,000 ksf (3,000,000 psi).

Theoretical vs Empirical Dead Load Deflections

Dead load deflections, as experimentally determined and as computed by the second and third methods, are listed in Table 1. Because the falsework was removed when the concrete was only 9 days of age, an elastic modulus of 288,000 ksf (2,000,000 psi) was used in the theoretical calculations.

Theoretical vs Empirical Live Load Moments

Figures 42 and 43 depict stress patterns computed by the second and third analytical methods for test vehicles in Positions 4.10 and 11.43, and 4.10 and 12.30, critical for center and exterior girders, respectively. These stresses were computed at the quarter-points, midpoints, and panel points of each slab using equations developed by Goldberg and Leve (4) for folded plates, for a 1,000-kip concentrated load moving transversely across the structure, and using the resulting influence lines in conjunction with a transparent overlay showing the test vehicle wheel locations in section. Mean stresses in each bay were computed by Simpson's rule, and these were used to compute internal resisting moments.

Resisting moments for the two conditions mentioned in the previous paragraph were also calculated by the first analytical method. Because resisting moments are the direct result of this method, the results for the 1,000-kip load were used to plot an influence surface, which was used in conjunction with a transparent overlay showing the test vehicle wheels in plan to determine moments as functions of transverse position of the left rear wheel. Results of these calculations are listed in Tables 13 through 24.

Theoretical vs Empirical Dead Load Moments

The theoretical dead load strain distribution, computed by the third analytical method, is depicted in Figure 44. Mean strains and stresses were computed for the gross concrete section for each half-bay by Simpson's rule and were used in computing dead load resisting moments, which are listed in Table 7.

A method of evaluation of the effects of slab cracking on load distribution is shown in Figure 45.

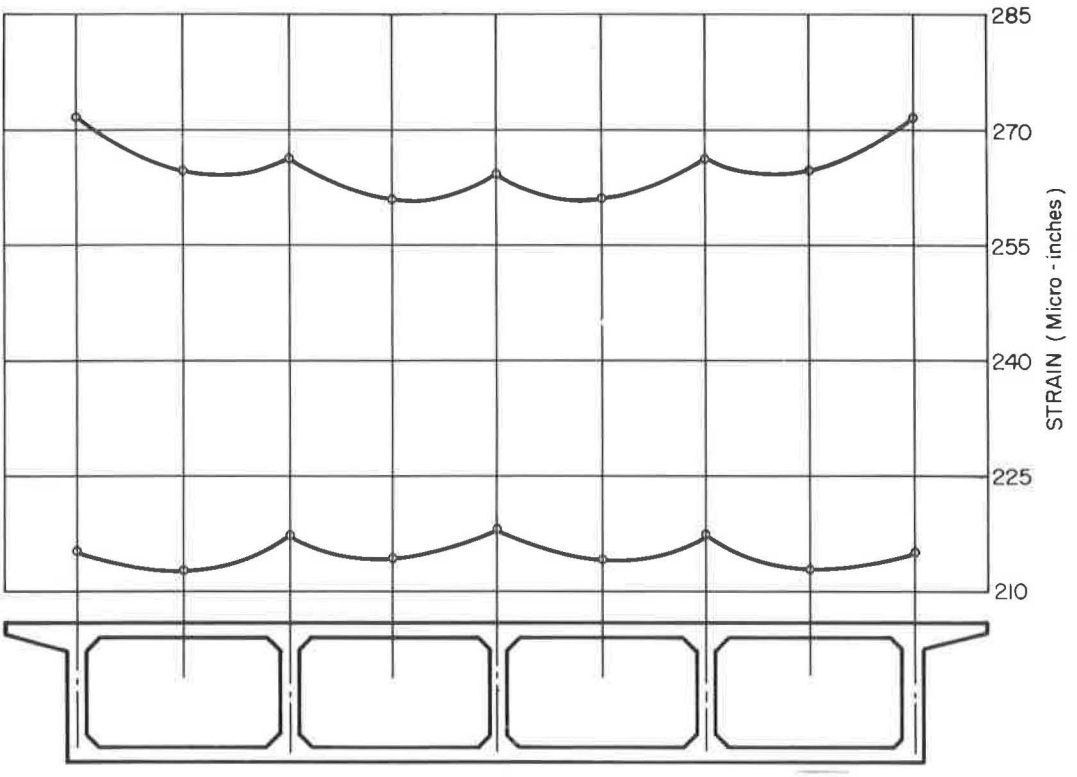

Figure 44. Theoretical dead load stress distribution computed by third method.

Figure 45. Cracking deck slab with 47-kip rear axle reaction on 10- by 14-in. plate to evaluate effects of slab cracking on load distribution.

Model Tests

Results of tests on plastic and concrete models by the University of California will be discussed in a separate report to be published at a future date.

CONCLUSIONS

The following conclusions may be drawn from studies of the results of testing the full-sized prototype:

1. Dead load deflections measured in the field agreed closely with those computed theoretically.
2. Correlation of total dead load resisting moments with known acting moments is good, provided that suitable modifications of concrete modulus are made to account for the effects of creep and shrinkage cracking. A satisfactory correlation exists among the ratios of individual stringer moments to the total resisting moment, based on 1961 AASHO specifications and similar ratios determined experimentally (Tables 5 and 6).
3. Live load distribution without an intermediate diaphragm indicated about 15 percent greater transverse distribution in the box girder than allowed in the 1961 AASHO specifications (Figs. 28 and 29). For this particular structure and test vehicle, the distribution factor determined experimentally approximated one-eighth of the stringer spacing.
4. Addition of a diaphragm at midspan resulted in a very small change in the distribution of moments across the transverse section; average change was 2 percent.
5. Addition of curbs and railings resulted in a large increase of total section stiffness. Changes in bottom main reinforcement strains were insignificant. Large reductions in top slab compressive strains were measured.
6. Theoretical analysis by the first method, in which the longitudinal stiffness of the structure is based on discrete stringer stiffnesses, thus neglecting the inherent longitudinal rigidity of the closed box section, is poor. This lack of correlation is more amply demonstrated by comparison of theoretical and empirical deflections in Figures 39, 40 and 41 than it is by consideration of Tables 13, 16, 17, 19, 22, and 23. The hypothetical placement of two trucks on the span in the latter calculation spreads the live loading over a relatively large proportion of the structure's width and tends to obscure the lack of consideration of torsional rigidity in this analytical approach.
7. The third analytical method did not accurately predict the patterns of transverse strain distribution in the deck slab or the lower layer of reinforcing steel for dead load (compare Figs. 21 and 22 with Fig. 34) or for live load (Figs. 37 and 38). However, when the theoretical or empirical strain patterns are used to compute stringer resisting moments, correlation between theoretical and experimental ratios is excellent (compare Tables 13 and 16 with 18, 19 and 22 with 24, and 5 with 7). This correlation is much poorer when the moments of the compressive resultants are taken about the tensile resultants (compare Tables 14 and 15 with 18, and 20 and 21 with 24).

ACKNOWLEDGMENTS

This research was financed in part with Federal-aid highway funds and was conducted with the approval of the U. S. Bureau of Public Roads. The work described herein was accomplished by the California Division of Highways, Bridge Department, of which J. E. McMahon is head. Instrumentation of the field prototype was accomplished by the California Division of Highways, Materials and Research Section, directed by F. N. Hveem. Professor A. C. Scordelis of the University of California furnished a valuable outline of possible analytical methods to be applied in studying behavior of the structure.

Acknowledgment is gratefully made to the following for their assistance in field work, data reduction and other services: H. R. Myers, William Chow, H. Bornhorst, J. Gates, J. Haug, P. Ibold, J. McKee, G. Matchette, A. Nelson, H. Stup, T. Suyetsugu, R. Tomlinson, J. Wing and J. Wyles, Violet Asano, Don Lancaster and the Judson Steel Corporation.

REFERENCES

1. Billig, Kurt. Structural Concrete. New York, St. Martins Press, 1960.
2. Hulsbos, C. L., and Linger, D. A. Dynamic Tests of a Three-Span Continuous I-Beam Highway Bridge. Highway Research Board Bull. 279, pp. 18-46, 1961.
3. Newmark, N. M. A Distribution Procedure for the Analysis of Slabs Continuous Over Flexible Beams. Univ. of Illinois Engineering Experiment Station, Bull. 304, June 17, 1938.
4. Goldberg, J. E., and Leve, H. L. Theory of Prismatic Folded Plate Structures. Publications, Int. Assoc. of Bridge and Structural Eng., Vol. 17, 1957.
5. Newell, J. S. Symmetric and Anti-symmetric Loadings. Civil Engineering, April 1939.
6. Holcomb, R. M. Distribution of Loads in Beam-and-Slab Bridges. Iowa Highway Research Board Bull. 12.